Published in final edited form as:
Nat Chem Biol. 2020 March ; 16(3): 327–336. doi:10.1038/s41589-020-0474-4.

Functional Dissection of the Retrograde Shiga Toxin Trafficking Inhibitor Retro-2

Alison Forrester[#1], **Stefan J. Rathjen**[#1], **Maria Daniela Garcia-Castillo**[#1], **Collin Bachert**[2], **Audrey Couhert**[3], **Livia Tepshi**[4], **Sylvain Pichard**[4], **Jennifer Martinez**[4], **Mathilde Munier**[3], **Raphael Sierocki**[4], **Henri-François Renard**[1], **César Augusto Valades-Cruz**[1], **Florent Dingli**[5], **Damarys Loew**[5], **Christophe Lamaze**[6], **Jean-Christophe Cintrat**[3], **Adam D. Linstedt**[2], **Daniel Gillet**[4,*], **Julien Barbier**[4], **Ludger Johannes**[1,*]

[1]Institut Curie, PSL Research University, Cellular and Chemical Biology unit, U1143 INSERM, UMR3666 CNRS, Endocytic trafficking and intracellular delivery team, Paris, France

[2]Department of Biological Sciences, Carnegie Mellon University, Pittsburgh, Pennsylvania, USA

[3]Service de Chimie Bioorganique et de Marquage (SCBM), CEA, Université Paris-Saclay, Gif-sur-Yvette, France

[4]Service d'Ingénierie Moléculaire des Protéines (SIMOPRO), CEA, Université Paris-Saclay, Gif-sur-Yvette, France

[5]Institut Curie, Centre de Recherche, PSL Research University, Laboratoire de Spectrométrie de Masse Protéomique, Paris, France

[6]Institut Curie, PSL Research University, Cellular and Chemical Biology unit, U1143 INSERM, UMR3666 CNRS, Membrane Dynamics and Mechanics of Intracellular Signaling team, Paris, France

[#] These authors contributed equally to this work.

[*]Correspondence to: ludger.johannes@curie.fr, Daniel.GILLET@cea.fr.

Data and code availability

The mass spectrometry proteomics data have been deposited to the ProteomeXchange Consortium via the PRIDE partner repository with the dataset identifier project accession PXD015642. Imaris and Matlab scripts for EEA1 quantification are available on request. The authors declare that all other data supporting the findings of this study are available within the paper and its supplementary information files.

Author contributions

LJ and DG conceived and designed the study. SJR, HFR, and MDGC performed click chemistry immunofluorescence, and MDGC and SJR click chemistry pull-down experiments. SJR performed in vitro Retro-2-pull-down, SNARE PLA, SNARE re-localization, Syn5-RUSH, and GPP130 rescue analysis. Intoxication assays were done by SJR, MDGC, JB and LT. BLI assay was performed by JB and RS. The purification of Syn5 and GPP130 variants, the monensin study and the *in vitro* Syn5-pull-down of the GPP130 variants were performed by CB and AL. SJR and MDGC performed Sec16A and syntaxin-5 proteomics analysis, immunofluorescence. AF performed the Sec23 kinetic studies, GFP-Sec16A pull-down, STxB, GPP130 and Syn5 immunofluorescence with quantification, and paper revisions. CAVC wrote the scripts and automated EEA1 colocalization methods. AC, MM and JCC designed and performed the chemical synthesis of azide-functionalized Retro-2 derivatives. JB and LT characterized their anti-Shiga toxin activity. JM, SP and LT prepared and characterized the recombinant $Sec16A_{1266\text{-}1678}$/Sec13 protein complex. FD carried out mass spectrometry work, DL supervised mass spectrometry and proteomic data analysis. SJR and LJ wrote the paper. AF, JCC, JB, DG, AL and CL critically revised the manuscript as well as aided in the design and analysis of experiments.

Competing Interests

The authors declare that there are no competing financial or non-financial interests in relation to the work described.

Abstract

The retrograde transport inhibitor Retro-2 has a protective effect on cells and in mice against Shiga-like toxins and ricin. Retro-2 causes toxin accumulation in early endosomes, and relocalization of the Golgi SNARE protein syntaxin-5 to the endoplasmic reticulum. The molecular mechanisms by which this is achieved remain unknown. Here, we show that Retro-2 targets the endoplasmic reticulum exit site component Sec16A, affecting anterograde transport of syntaxin-5 from the endoplasmic reticulum to the Golgi. The formation of canonical SNARE complexes involving syntaxin-5 is not affected in Retro-2-treated cells. In contrast, the interaction of syntaxin-5 with a newly discovered binding partner, the retrograde trafficking chaperone GPP130, is abolished, and we show that GPP130 must indeed bind to syntaxin-5 to drive Shiga toxin transport from endosomes to the Golgi. We thereby identify Sec16A as a druggable target, and provide evidence for a non-SNARE function for syntaxin-5 in interaction with the GPP130.

Keywords

Retrograde transport; STxB; Shiga toxin; Shiga-like toxin; Retro-2; chemical genetics; chemical biology; syntaxin-5; Sec16A; GPP130; click chemistry; small molecule; mass spectrometry; SNARE; trans-Golgi network; COPII; anterograde trafficking; proximity ligation assay; retention using selective hooks

Introduction

Shigella dysenteriae and enterohemorrhagic strains of *Escherichia coli* (EHEC) produce the bacterial Shiga toxin and Shiga-like toxins (SLT), respectively[1]. SLTs, especially from *E. coli* strain O157:H7 and other serotypes, are responsible for pathological manifestations that can lead to hemolytic-uremic syndrome (HUS), the leading cause of pediatric renal failure in the world. The most life-threatening extra-intestinal disease manifestations include renal failure and central nervous system complications. To date, no specific treatment options exist, and clinical management of HUS remains purely supportive[2].

Shiga toxin and the SLTs are type 2 ribosome inactivating proteins with an AB_5 type molecular structure. The catalytic A-subunit is responsible for the cleavage of an adenine base on position 4,324 of the 28S ribosomal RNA (rRNA)[3]. The A-subunit is non-covalently associated with the homopentameric B-subunit (STxB)[4]. STxB binds the cellular toxin receptor, a glycosylated lipid termed globotriaosylceramide (Gb3, or CD77), with 15 Gb3 binding sites per STxB homopentamer[5]. After receptor binding, Shiga toxin is internalized by clathrin-dependent[6] and independent[7] endocytosis. From early/maturing endosomes, the toxin is then transported via the retrograde route to the *trans*-Golgi network (TGN)[8] and the endoplasmic reticulum (ER)[9], from where the catalytic A-subunit is translocated to the cytosol[10]. The bacterial cholera toxin and the plant toxin ricin share with Shiga toxin the capacity to undergo retrograde transport from the plasma membrane to the ER[11, 12].

Retrograde sorting of Shiga toxin on early and maturing endosomes has been extensively studied[11, 12]. Key retrograde machinery includes Rab6 (Ref.[8]), the retromer complex[13–15],

and GPP130 which was shown to be involved in retrograde transport of Shiga toxin and SLT1 (Ref.[16]), but not that of SLT2 (Ref.[17]).

Two SNARE complexes have been implicated in Shiga toxin trafficking from early/maturing endosomes to the Golgi apparatus: one composed of syntaxin-16, syntaxin-6, Vti1, and VAMP4 (Ref.[8]), and a second composed of syntaxin-5 (Syn5), GS28, Ykt6, and GS15 (Ref.[18]). While VAMP4 is clearly localized on early endosomes and functions as a vSNARE for fusion of endosomal retrograde transport carriers with TGN membranes, the constituents of the Syn5/GS28/Ykt6/GS15 complex are solely Golgi-localized. Syn5 has been described to cycle between the Golgi and the ER[19], involving COPII vesicles for its anterograde transport in a complex with Syn5 itself and the alternative SNARE partners GS27/SEC22/BET1 (Ref.[20]). The discovery of two SNARE complexes that are involved in retrograde early/maturing endosomes-to-TGN Shiga toxin trafficking thus raises the question as to their true function in retrograde sorting and the exact mechanism by which they regulate this transport step.

Several small molecule inhibitors have been developed against Shiga toxin and ricin[21, 22]. The Retro compounds have been shown to protect mice against lethal challenges by ricin[23], or by SLT2 produced by the *E. coli* strain O104:H4 (Ref.[24]). Furthermore, these compounds also possess protective activity against pathogens as diverse as *Leishmania* species, enterovirus 71, herpes-, cytomegalo-, polyoma-, papilloma-, filo-, poxviruses, and Chlamydiales [25–33]. A Retro-2 variant with improved activity, termed Retro-2.1, was recently obtained in structure-activity relationship studies[28, 34], enabling downstream target identification experiments described herein.

At the cellular level, Retro-2 leaves compartment morphology intact, but induces the redistribution of Syn5 from the Golgi apparatus to the ER, and the accumulation of Shiga toxin in early endosomes[23]. Whether and how these events are linked has remained unexplored.

In this study, we used biorthogonal click chemistry coupled to mass spectrometry to search for Retro-2 interacting partners. The ER exit site (ERES) component Sec16A was identified as a top hit. Our data show that in agreement with an effect on Sec16A activity, Retro-2 treatment leads to a partial redistribution of Syn5 to the ER by reducing the COPII-dependent anterograde flow of the SNARE protein as it recycles through the ER[19]. Under these conditions, the newly discovered interaction of Syn5 with the Shiga toxin trafficking chaperone GPP130 is abolished, and we furthermore demonstrate in mutational studies that the interaction capacity of Syn5 with GPP130 is required for the latter to drive retrograde early/maturing endosomes-to-Golgi trafficking of Shiga toxin.

In conclusion, a model emerges from our study in which the site of action of Retro-2 in the ER is linked with the site of toxin accumulation in early endosomes. Furthermore, we provide evidence for a non-SNARE function of Syn5 as an interactor of GPP130. By identifying Sec16A as a key target of Retro-2, our findings lay the foundation for structure-based optimization of the compound as a broad spectrum inhibitor of intracellular toxins and pathogens.

Results

Retro-2 targets the ER exit site

To identify the intracellular targets of Retro-2, a clickable fully active version of the inhibitor based on optimized Retro-2.1 (compound **1**) was obtained (Fig. 1a; compound **2**, see **Synthetic Procedures** in Supplementary Notes for synthesis). Clickable Retro-2.1 was incubated for 30 min at 37 °C with HeLa cells, bioorthogonally reacted with a biotin compound (compound **3**), and after cell lysis pulled down on streptavidin-beads. By mass spectrometry, the ERES component Sec16A was identified as a top hit (Supplementary Table 1 shows one representative experiment of two; see Methods for link to full data set). This interaction was confirmed in western blotting experiments (Fig. 1b,c). Binding specificity was documented by pull-down experiments in the presence of a 5-fold molar excess of non-clickable Retro-2.1. In this competition condition, the Sec16A signal was strongly reduced (Fig. 1b,c and Supplementary Table 1).

Sec16A (250 kDa) has not yet been purified as a full-length protein. In yeast, a partial fragment corresponding to amino acids 1266-1678 of human Sec16A has been purified in interaction with its binding partner Sec13 (Ref.[35]). For the current study, human $Sec16A_{1266\text{-}1678}$/Sec13 complex was therefore expressed in and purified from *E. coli* (see Methods) to be used in pull-down experiments with clickable Retro-2.1 coupled *in vitro* to biotin (compound **3)** or a fluorophore (compound **4**) (Fig. 1a). This biotinylated version of Retro-2.1 (compound **5)**, was bound to Streptavidin beads to saturation, which were then incubated with purified $Sec16A_{1266\text{-}1678}$/Sec13. Streptavidin beads saturated with biotin alone were used as controls. Western blot analysis of bead-associated proteins revealed that Retro-2.1 interacts directly with $Sec16A_{1266\text{-}1678}$/Sec13 (Supplementary Fig. 1a,b). Furthermore, upon competition with a 5-fold excess of un-clickable Retro-2.1, the pull-down signal was diminished to background levels (Supplementary Fig. 1a,b), strongly supporting the specificity of the direct interaction between Retro-2 and $Sec16A_{1266\text{-}1678}$/Sec13.

The kinetic constants of this interaction were measured by bio-layer interferometry (see Supplementary Fig. 1c for the experimental setup). The K_D of Retro-2.1 for Sec16A was in the nM range (Fig. 1d and Supplementary Fig. 1d).

The clickable version of Retro-2.1 was then used for bioorthogonal labeling with a fluorophore to document its intracellular distribution (compound **6**). Under control conditions (scrambled siRNA transfection), Retro-2.1 localized to dotted perinuclear structures (Fig. 1e, top image). Upon depletion of Sec16A using siRNAs, Retro-2.1-specific labeling was strongly diminished (Fig. 1e, bottom image). The quantification of fluorescence intensities showed a strong reduction of Retro-2.1 labeling to 21.5 ± 6.2% in Sec16A-depleted cells (Fig. 1f), demonstrating that Sec16A expression was needed for Retro-2.1 binding in cells.

Depletion of Sec16A phenocopies Retro-2 treatment

One of the salient features EEA1-labeled of Retro-2 treatment is the inhibition of retrograde transport of STxB between early/maturing endosomes and the TGN[23]. Upon incubation of STxB with HeLa cells for 45 min at 37 °C, the depletion of Sec16A led to a reduced

accumulation of STxB (red) in the Golgi (labeled with giantin, green, Fig. 2a), and an increased localization of STxB to endosomes (blue in right panels of Fig 2a). These effects were quantified by measuring the fluorescence signal of STxB within the Golgi region, as marked by anti-giantin immunolabeling, over total cellular STxB fluorescence signal (Fig. 2b), or by counting the number of EEA1 positive spots that were also positive for STxB (Fig. 2c; see Methods for details).

The depletion of the second and third Retro-2.1 interaction candidates from the pull-down experiment (Supplementary Table 1), i.e. mitogen-activated protein kinase kinase kinase 5 (MAP3K5) and neurofibromin (NF1), a regulator of the MAP kinase pathway, slightly increased the presence of STxB in EEA-positive endosomes (Supplementary Fig. 2a,c), without affecting the protein's accumulation in the Golgi (Supplementary Fig. 2a,b). A small effect on STxB trafficking when interfering with the mitogen-activated kinase pathway is consistent with previous findings on the dependency of Shiga toxin trafficking on mitogen-activated protein kinase p38 (Ref.[36]).

Retro-2 treatment protects cells from intoxication by Shiga toxin measured via the incorporation of radiolabeled methionine into newly synthesized proteins[23]. Similar to Retro-2 treatment, depletion of Sec16A resulted in a 3.9 ± 1.1-fold protection (Fig. 2d shows one representative experiment out of 3, note that Retro-2 and Sec16A curves overlap), suggesting less efficient transport along the retrograde route to the ER from where the catalytic A-subunit then translocates to the cytosol.

Retro-2 induces the redistribution of Syn5 to the ER[23]. Interestingly, Syn5 was not found amongst the presumed Retro-2.1 interacting partners from the pull-down experiment (see Methods for link to full data set), suggesting that its relocalization from the Golgi to the ER may be an indirect effect of the drug treatment (see below). We found that this phenotype was reproduced upon depletion of Sec16A (Fig. 2e; note the increased peripheral Syn5 (red) labeling in Retro-2-treated or Sec16A-depleted cells; Golgi labeled with TGN46 (green)). Quantification showed that the effect on Syn5 localization to the Golgi was similar for Retro-2 treatment and Sec16A depletion (Fig. 2f).

Taken together with the interaction and localization data of Fig. 1, these findings support the idea that Sec16A is a cellular target of Retro-2.

Retro-2 slows the anterograde transport of Syn5

As part of the ERES machinery, Sec16A functions in the biosynthetic/secretory transport of proteins from the ER. To test whether Retro-2 affects the anterograde transport of Syn5, we adapted the retention using selective hook (RUSH) approach to study this SNARE (see Methods). We fused Syn5 to the streptavidin-binding peptide (SBP) and eGFP, and co-expressed a KDEL-core-streptavidin fusion protein, which causes the retention of Syn5-SBP-eGFP in the ER. After addition of biotin, Syn5-SBP-eGFP is released from the ER and traffics to the Golgi apparatus. Giantin was used to define the Golgi apparatus in immunofluorescence experiments, and the fraction of Syn5-SBP-eGFP in the Golgi was determined. In control conditions, more than 90% of Syn5 was found in the Golgi apparatus within 20 min of biotin addition (Fig. 3a; quantification in Fig. 3b). Upon Retro-2 treatment,

this fraction was reduced to 68.2 ± 5.3% (Fig. 3a,b; note the increase of peripheral ER labeling of Syn5 in the Release+Retro-2 condition). In contrast, the anterograde trafficking of mannosidase II (ManII) (Fig. 3c; quantification in Fig. 3d), was not affected by Retro-2 treatment.

In the light of the observed specificity of Retro-2 on the anterograde transport of Syn5, we hypothesized that the compound might not affect general COPII dynamics at ERES. To test this, fluorescence recovery after photobleaching (FRAP) experiments were performed on an essential COPII component, Sec23A, to analyze changes in ERES cycling efficiency and thus perturbation of ERES function. HeLa cells transiently expressing GFP-Sec23A were incubated with Retro-2, or depleted of Sar1A/B, a GTPase critical for COPII vesicle formation. After photobleaching, fluorescence recovery signal and half-life ($t_{1/2}$) of fluorescence recovery (Supplementary Fig. 3a,b) were quantified. As expected[37], Sar1A/B depletion significantly slowed recovery with half-lives ranging from 7.5 s in control conditions to 9.6 s in Sar1A/B depleted cells (Supplementary Fig. 3b). In contrast, in Retro-2-treated cells no statistically significant change was measured (Supplementary Fig. 3b), demonstrating that Retro-2 did not have a general effect on COPII dynamics. The immobile fraction was also unchanged by Retro-2 treatment (Supplementary Fig. 3c,d).

The Retro-2 effect on trafficking was surprisingly specific for Syn5, without affecting other cargoes or overall ERES dynamics. We addressed whether general interference with ERES would in return have an effect on STxB trafficking. For this, Sar1A/B was depleted from HeLa cells (see Supplementary Fig. 3b for effect on COPII dynamics), and STxB transport was assayed. STxB arrival at the Golgi was found to be decreased under these conditions, and retention in endosomes increased (Fig. 3e-g). These findings confirmed the link between ERES dynamics and STxB trafficking.

To get first indications on how Retro-2 might influence Sec16A function at ERES, we performed GFP-Sec16A pull-down in the presence and absence of the optimized compound Retro-2.1. After mass spectroscopy analysis, we identified a list of proteins whose interaction with Sec16A is significantly decreased in Retro-2.1 treatment conditions (Supplementary Fig. 4, complete lists after quantification in Supplementary Datasets 1 (Sec16A interactome) and **2** (Sec16A interactome +/- Retro-2), and PRIDE data repository as indicated in Methods section). Of note, several of these fall into the general gene ontology categories “cargo loading into COPII vesicles” (including Sec13, Sec23A,B, and Sec24A-C), and “Golgi vesicle transport” (Supplementary Fig. 4). These findings provide leads for future exploration of the detailed molecular and atomistic mechanisms of Retro-2.1 function.

Our results suggest that the redistribution of Syn5 to the ER upon incubation of cells with Retro-2 results from a reduced rate of anterograde ER-to-Golgi transport of the protein. This effect appears to be specific for Syn5, as one other endogenous cargo (this study) and one heterologous[23] were not affected by compound treatment. The molecular reasons for this specificity remain to be fully explored at this stage, but likely involve a subtle modulation of Sec16A interaction with the COPII machinery.

Syn5 SNARE complexes are unaltered by Retro-2 treatment

Syn5 forms two Golgi-localized SNARE complexes: Syn5/GS27/Bet1/Sec22b at the cis-Golgi, and Syn5/GS28/Ykt6/GS15 at medial-to-trans-Golgi[38–41]. A function of the latter in endosomes-to-Golgi trafficking of Shiga toxin has been suggested[18]. We therefore analyzed whether these Syn5 SNARE partners were also relocalized upon Retro-2 treatment. Localization of Syn5, GS27, and GS28 in the Golgi area was determined as described for Fig. 2a. Remarkably, the Golgi fraction of GS27 and GS28 remained unaltered upon Retro-2 treatment, whereas the Golgi fraction of Syn5 was reduced by approximately half (Fig. 4a,b; note the increase of peripheral ER labeling of Syn5 in the Retro-2 condition in Fig. 4a, bottom panel). Thus, the Retro-2-induced relocalization effect was limited to Syn5.

The proximity ligation assay (PLA) was used to analyze the co-distribution of Syn5 with its SNARE partners GS27 or GS28 on a nanometric scale. The number of PLA dots per μm^2 was not affected by the incubation of cells with Retro-2 (Fig. 4c,d), suggesting that despite the partial relocalization of Syn5 under these conditions (Fig. 4a,b), Syn5 containing SNARE complexes remain unaltered.

This was tested directly in co-immunoprecipitation experiments. HeLa cells were transfected with GFP-tagged Syn5 and co-immunoprecipitated proteins were analyzed by western blotting. The levels of GS27 and GS28 that were co-immunoprecipitated with GFP-Syn5 were not affected by incubation of cells with Retro-2.1 (Fig. 4e), demonstrating that the Syn5-containing SNARE complexes remained unaltered in the presence of the drug.

Several convergent lines of evidence thus suggest that despite the partial relocalization of Syn5 to the ER, the formation of its SNARE complexes is not affected. It therefore appears unlikely that the inhibition of retrograde transport of Shiga toxin from endosomes to the Golgi that is observed in Retro-2-treated cells[23] is due to an altered SNARE function.

Syn5 binds to GPP130

In co-immunoprecipitation experiments followed by mass spectrometry analysis we found the Golgi integral membrane protein 4 (GPP130 or GOLIM4) amongst the interacting partners of GFP-Syn5 (Supplementary Fig. 5 for volcano plot, Supplementary Table 2, Supplementary Dataset 3 for quantification, and Methods for a link to full list of interacting proteins). This was compelling as GPP130 not only cycles between TGN, plasma membrane, and endosomes[42], but also functions in Shiga toxin trafficking between endosomes and the TGN[16, 43]. The interaction between Syn5 and GPP130 was confirmed by western blotting of proteins that were co-immunoprecipitated with Syn5 (Fig. 5a,b). Importantly, upon treatment of cells with Retro-2 or the optimized Retro-2.1, the co-immunoprecipitation of GPP130 with GFP-Syn5 was reduced or lost, respectively (blot in Fig. 5a; quantification from 4 independent experiments in Fig. 5b). As controls, we show that siRNA-mediated depletion of GPP130 or Syn5 also led to a loss of the GPP130 signal from the immunoprecipitation pellet (Fig. 5a).

Syn5 has a luminal domain of only one amino acid. GPP130 is localized at the cis/medial-Golgi, and has a large C-terminal luminal domain, a trans-membrane domain, and a small 12 amino acid cytosolic N-terminal domain[44]. It therefore seems likely that the interaction of

Syn5 with GPP130 occurs via the trans-membrane and/or cytosolic domains of both proteins (Fig. 5c). To test this hypothesis, the GST-tagged cytosolic transmembrane domain of GPP130 (residues 1-108; blue in Fig. 5c) and the 6xHis cytosolic-transmembrane domain of Syn5 (residues 202-355; green in Fig. 5c) were purified, and pull-down assays were performed on glutathione beads. Proteins from the pull-downs were quantified by Coomassie blue staining of SDS-PAGE gels (Fig. 5d). Wild-type GST-tagged GPP130 fragment 1-108 bound 30.5 ± 7.9% of Syn5 fragment 202-355 that was present in the incubation (Fig. 5d). Non-fused GST, the GST-tagged GPP130 cytosolic domain mutant $KR_{11,12}AA$, and a GST-tagged chimera in which the cytosolic domain of GPP130 was replaced by an unrelated sequence from the cytosolic domain of the dipeptidyl peptidase-4 (termed DGG) were included in this analysis. These proteins only bound respectively, 2.6 ± 1.4%, 4.8 ± 1.2%, or 5.4 ± 1.2% of Syn5 fragment 202-355 (Fig. 5d), which documented the specificity of our finding of a direct interaction of $GPP130_{1\text{-}108}$ with $Syn5_{202\text{-}355}$.

The presence of Retro-2 in the incubation mix did not affect the interaction of $GPP130_{1\text{-}108}$ with $Syn5_{202\text{-}355}$ (Fig. 5e), which is in contrast to the strongly reduced co-immunoprecipitation of both proteins from cells under these conditions (Fig. 5a,b; see discussion). The *in vitro* result is in agreement with the absence of Syn5 and GPP130 from the list of presumed Retro-2 interacting partners (see Methods for link to full data set).

We therefore concluded that the interaction between GPP130 and Syn5 is direct, efficient, abolished by the $KR_{11,12}AA$ mutation on GPP130, and insensitive to Retro-2 on purified proteins, while it is prevented by Retro-2 treatment within the cellular context (see discussion).

Syn5-GPP130 interaction is required for STxB trafficking

To test the functional importance of the GPP130-Syn5 interaction, GPP130 was depleted from HeLa cells, which were then transfected with wild-type GPP130 or the $KR_{11,12}AA$ mutant prior to measuring STxB trafficking from the plasma membrane to the Golgi apparatus. Upon incubation for 45 min at 37 °C, 86,4 ± 1,5% of STxB reached the Golgi area under control conditions (Fig. 6a). GPP130 depletion using siRNAs reduced the Golgi fraction of STxB to 63.2 ± 2.5%. Upon re-transfection of wild-type GPP130, this value increased to 83.2 ± 1.8%, indicating that GPP130 activity was efficiently rescued. In contrast, when the $KR_{11,12}AA$ construct was expressed to wild-type levels, only 57.1 ± 4% of STxB was found in the Golgi area, which is similar to GPP130 depletion conditions (Fig. 6a). The $KR_{11,12}AA$ mutant protein thus failed to rescue GPP130 function in retrograde trafficking of STxB, indicating that its interaction with Syn5 is required for this activity.

Monensin has been described to disperse TGN network determinants[45] due to its ionophoric properties[46]. In monensin-treated cells, wild-type GPP130 and the $KR_{11,12}AA$ mutant relocalized from the Golgi area (Fig. 6b, top row) to endosomal structures (Fig. 6b, middle row). Within 3 hours of monensin wash-out, the majority of wild-type GPP130 was localized back to the Golgi area, whereas the majority of $KR_{11,12}AA$ mutant molecules were still present in endosomal or intermediate structures (Fig. 6b, bottom row; quantification in Fig. 6c), strongly suggesting that retrieval was delayed. These findings demonstrate again that the Syn5 interaction domain of GPP130 was critical for its activity.

We finally found that GPP130 distribution was altered by interference conditions that affect STxB trafficking from early/maturing endosomes to the Golgi: GPP130 localization to the Golgi apparatus was reduced in Sec16A or Sar1A/B depletion conditions (Fig. 6d,e), and its overlap with EEA1 was increased (Fig. 6d,f).

Discussion

Studies in mice have shown that the small molecule inhibitor Retro-2 protects against the plant toxin ricin[23] and bacterial SLT[24]. On cells, the compound also shows activity against other intracellular pathogens[25–33]. However, the molecular mechanism of action of Retro-2 remained unknown. Using biorthogonal click-chemistry[47], we have identified the ERES component Sec16A as a direct molecular target of Retro-2. The function of Sec16A in the anterograde transport of the Golgi SNARE protein Syn5 appears to be specifically disrupted by Retro-2, thereby resulting in the partial relocalization of Syn5 to the ER. Concomitantly with this relocalization, the newly identified interaction of Syn5 with the endosomal cycling protein and Shiga toxin trafficking chaperone GPP130 is lost. As Retro-2 does not affect the direct binding of Syn5 to GPP130, it is concluded that the loss of interaction in cells is due to the relocalization of Syn5. Further experiments show that the Syn5-GPP130 interaction is required for efficient Shiga toxin trafficking from early endosomes to the Golgi. Our study thereby provides a model to explain the surprising observation that Retro-2, by acting on the ER-localized Sec16A, diminishes Shiga toxin trafficking from early endosomes to the Golgi apparatus (Fig. 6g). Since Retro-2 does not affect the SNARE complexes in which Syn5 is involved, our study further suggests a non-SNARE function of Syn5 via its interaction with GPP130 at the early/maturing endosomes-TGN interface.

The identification of Sec16A as a cellular target of Retro-2 is a key discovery of our study. We thereby highlight this ERES component as a trafficking factor whose molecular characteristics can be tuned by small molecules such as to remain permissive for cellular functions while restricting pathogen progression sufficiently to allow for countermeasures of the host to be efficient. We expect that this finding will pave the path for the development of anti-pathogen intervention strategies, based on Retro-2 and beyond.

Since Syn5 has been shown to bind to Sec24C/D isoforms[48], and Retro-2 treatment interferes with the interaction of Sec16A with Sec23 and Sec24 isoforms (this study), it might be speculated that the specific effect on anterograde Syn5 trafficking that is observed in the presence of the drug originates from differential dependency of cargoes on subtle changes in COPII dynamics at ER exit sites. In agreement with this interpretation, we have found that the overall dynamics of COPII at ER exit sites is not significantly perturbed by the compound. Other possibly complementary interpretations are that the multi-domain nature of Sec16A[49] mediates functionally distinct interactions with diverse cargoes, and/or that different cargoes have different cycling kinetics. Further studies are needed to differentiate between these options.

Our initial hypothesis was that Syn5 itself was the target of Retro-2 and that its effect on Shiga toxin trafficking was the result of perturbed SNARE function. It was therefore a surprise when several convergent lines of evidence led to the conclusion that the integrity of

Syn5 SNARE complexes was not affected under Retro-2 treatment conditions. These findings on unperturbed SNARE complex formation appear to be in contradiction with the 50% reduction of Syn5 localization at the Golgi in Retro-2-treated cells. The remaining 50% of Golgi-localized Syn5 is apparently sufficient to maintain SNARE activity.

The interaction between Syn5 and the cis-Golgi cycling protein GPP130 represents another key discovery of our study. A function in Shiga toxin trafficking has previously been established for GPP130 (Ref.[16, 43]), and our mutational studies indicate that GPP130 must indeed bind to Syn5 to function in retrograde sorting. Since binding occurs at the level of the cytosolic domains, one might invoke a trans-interaction between both proteins on opposing membranes. Yet, a role in tethering appears unlikely when one considers the short length of GPP130's cytosolic domain. The interaction between both proteins could also occur in *cis* on the same membrane, for example for sorting in endosomes.

On cells, Retro-2 treatment leads to a loss of GPP130 from the pellet of proteins that are co-immunoprecipitated with Syn5. In contrast, Retro-2 does not affect the direct *in vitro* interaction between both proteins. The most likely interpretation of the cellular data is that the loss of interaction under Retro-2 incubation conditions results from the relocalization of Syn5 away from a Golgi subcompartment into which it is normally codistributed with GPP130. The unperturbed Golgi SNARE complex interactions of Syn5 might then occur in a different Golgi subcompartment. The difficulty with quantitatively studying the intra-Golgi distribution of proteins renders it challenging to address this hypothesis experimentally.

GPP130 only binds to Shiga toxin and SLT1, and not to SLT2 (Ref.[17]), while Retro-2 protects against all these toxins[23]. We hypothesize that SLT2 may bind to other chaperoning proteins whose retrograde trafficking might also depend on their interaction with Syn5.

In conclusion, our study provides a mechanistic model on how Retro-2 affects Shiga toxin trafficking at the level of early endosomes by acting on the ER protein Sec16A. A non-SNARE function for Syn5 as an interactor of GPP130 emerges as a novel modality for the regulation of retrograde trafficking at the endosomes-TGN interface.

Online Methods

Cell lines

HeLa cells were maintained at 37 °C under 5% CO2 in DMEM/GlutaMAX©/4,5 mg/mL glucose (Invitrogen, Waltham, MA, USA), supplemented with 10% heat-inactivated fetal bovine serum (Invitrogen, origin: Australia), 0.01% penicillin-streptomycin (Invitrogen), and 1 mM pyruvate (Invitrogen). For SLT1 intoxication studies, a HeLa cell clone was selected for homogenous Gb3 expression and cultured as above. A stable cell line expressing GFP-Syn5 fusion protein was produced from HeLa cells, and was cultured as above, including 0,5 mg/mL G418. GFP-Syn5 cells were used for the Syn5 immunoprecipitations.

Antibodies and reagents

Antibodies against the following antigens were purchased from the indicated sources: Syn5 (Synaptic Systems, Cat#110053), GFP, giantin (institutional antibody platform at Curie

Institute), TGN46 (BioRad, Cat#AHP500GT) GS27, GS28 (both BD Biosciences; Cat#611034, and Cat#611184), Sec16A (Proteintech Europe, Cat#20025-1-AP). Anti-GPP130 was produced in the Linstedt lab. Fluorescent tagged secondary antibodies were purchased from Beckman Coulter and used at 1:400 dilution: Donkey anti-Mouse Cy3 (catalogue #715166150, lot 129511), donkey anti-mouse FITC (catalogue #715196150, lot 92566), donkey anti-rabbit Cy3 (catalogue #111166045, lot 122096), donkey anti-rabbit FITC (catalogue #711096152, lot 85714), donkey anti-goat 647 (catalogue #705605147, lot 128808), donkey anti-goat Cy3 (catalogue #705166147, lot 126500), donkey anti-sheep Cy3 (catalogue #713166147, lot 106361). HRP-tagged antibodies were also purchased from Beckman Coulter and used at a dilution of 1:2000: Donkey anti-rabbit (catalogue #711035152, lot 136860), donkey anti-mouse (catalogue #715038151, lot 133192). Pre-cast SDS-PAGE gels were purchased from BioRad. The following plasmids were gifts from the indicated researchers: Syn5-EGFP (Jeffrey E. Pessin, The University of Iowa, USA), Sec16A-GFP (David Stephens, University of Bristol, England), RUSH constructs and mCherry-KDEL (Franck Perez, Curie Institute, Paris, France), GFP-Sec23A (Antonella De Matteis, TIGEM, Naples, Italy). STxB-Cy3 was produced as described[51].

RNA interference

siRNAs against Sec16A, MAP3K5, NF1, Sar1A, Sar1B, Syn5 or GPP130 were purchased from Qiagen (minimum of two different oligonucleotides). Scrambled siRNAs were used as control. 150,000 HeLa cells were plated overnight in 35 mm well dishes (6 well plates), and transfected with 25 pmol siRNA, 7.5 µl Lipofectamine® RNAiMAX transfection reagent (Invitrogen). Experiments were performed 72 h after transfection. Decreased expression levels were confirmed by western blotting.

Calcium phosphate–DNA co-precipitation

HeLa cells were plated overnight in complete medium supplemented with 25 mM HEPES (pH 7.2 – 7.4) to reach a confluency of 50-80%. A solution of 10 µL of 2.5 M $CaCl_2$ and the optimized amount of plasmid DNA were diluted in 90 µL TE buffer (1 mM Tris–HCl, 0.1 mM EDTA, pH 7.6) to a final volume of 100 µL. The Ca/DNA/TE mix was added dropwise to an equal volume of 2x HeBS solution (160 mM NaCl, 1.5 mM Na_2HPO_4, 50 mM HEPES, pH 7.05 at 23 °C). This transfection solution was added dropwise onto cells in a 1:10 dilution[52].

Retro-2 treatment

Retro-2 (2-([(5-methyl-2-thienyl)methylene]amino)-N-phenylbenzamide) was purchased from Sigma Aldrich (St. Louis, MO, USA) and stored at 50 mM in DMSO at -20 °C. Cells were pre-treated at 37 °C with 25 µM Retro-2 in complete growth medium, either 30 min for Shiga toxin intoxication and STxB trafficking experiments, or 60 min for the Syn5-RUSH assay or Syn5 co-immunolabeling experiments. DMSO at a concentration of 0.05% in complete growth medium was used as control. Treatment of cells with optimized Retro-2.1 (synthesis described in Supplementary Notes, compound **1**), like Retro-2, was at 37 °C with 25 µM Retro-2.1 in DMSO.

Sec16A$_{1266-1678}$/Sec13 production

Human Sec16A (residues 1266–1678) and Sec13 were cloned into a bicistronic pET-Duet vector. The complex Sec16A$_{1266-1678}$/Sec13 has a Strep Tag (in bold) at the N-terminus of Sec13 (M**WSHPQFEK**SAMVSVINTVDTSHEDMIHDAQMDYYGTRLATCSSDRSVKIFDVRN GGQILIADLRGHEGPVWQVAWAHPMYGNILASCSYDRKVIIWREENGTWEKSHEHA GHDSSVNSVCWAPHDYGLILACGSSDGAISLLTYTGEGQWEVKKINNAHTIGCNAVS WAPAVVPGSLIDHPSGQKPNYIKRFASGGCDNLIKLWKEEEDGQWKEEQKLEAHSD WVRDVAWAPSIGLPTSTIASCSQDGRVFIWTCDDASSNTWSPKLLHKFNDVVWHVS WSITANILAVSGGDNKVTLWKESVDGQWVCISDVNKGQGSVSASVTEGQQNEQ) and a 6xHis tag (in bold) at the N-terminus of Sec16A (MGSS**HHHHHH**SKFSVPHVCARFGPGGQLIKVIPNLPSEGQPALVEVHSMEALLQHT SEQEEMRAFPGPLAKDDTHKVDVINFAQNKAMKCLQNENLIDKESASLLWNFIVLL CRQNGTVVGTDIAELLLRDHRTVWLPGKSPNEANLIDFTNEAVEQVEEEESGEAQLS FLTGGPAAAASSLERETERFRELLLYGRKKDALESAMKNGLWGHALLLASKMDSRT HARVMTRFANSLPINDPLQTVYQLMSGRMPAASTCCGDEKWGDWRPHLAMVLSN LNNNMDVESRTMATMGDTLASRGLLDAAHFCYLMAQAGFGVYTKKTTKLVLIGSN HSLPFLKFATNEAIQRTEAYEYAQSLGAETCPLPSFQVFKFIYSCRLAEMGLATQAFH YCEAIAKSILTQPHLYSPVLISQLVQMASQLR). The plasmid construct was ordered from GeneArt (ThermoFisher Scientific).

The complex of proteins was expressed in *E. coli* strain Shuffle T7 Express (New England BioLabs) in Luria-Bertani medium with 30 μg/mL kanamycin, induced with 1 mM isopropyl-β-d-1-thiogalactopyranoside (Sigma) at 30 °C. Harvested cells were homogenized (Emulsiflex C3, Avestin) at 4 °C in 50 mM potassium phosphate, pH 8.5, 400 mM NaCl, 2.5 mM desthiobiotin, and 5 mM β-mercaptoethanol supplemented with 1 mM PMSF, 10 mM $MgCl_2$, and 25 U/mL benzonase. The Sec16A$_{1266-1678}$/Sec13 complex was purified on Strep-Trap HP 5 mL. Sec16A$_{1266-1678}$/Sec13 was concentrated to 3.2 mg/mL. The level of protein expression and purity were analyzed by spectrophotometry, Laemmli SDS-PAGE and western blotting (Supplementary Fig. 6).

GPP130 – Syn5 interaction

Constructs—His-Syn5ΔNT was constructed by placing residues 201-355 in frame with a 6xHis tag in pRSET-B. GST-TEV-GPP130 (1-108) was made from an existing construct of GST-TEV-GPP130 (1-248) in pGEX-2T by PCR mutagenesis creating a stop codon after residue 108 (GST-TEV-GPP130 junctions: …PPKSDLVPRGS-ENLYFQGSSGA-MGNGMCSRKQKR…). GST-TEV-GPP130 (1-108) with DPPIV's cytoplasmic domain replacing that of GPP130 was made by a loop-in replacement PCR strategy. GPP130-GFP was made by cloning GPP130 into the pEGFP vector. KR-mutants were made by PCR mutagenesis.

Protein purification—A 25 mL BL21 starter culture was used to inoculate a liter culture at 37 °C. Cells were grown to an O.D. of 0.6 at 600 nm. Temperature was reduced to 18 °C, and cells were incubated with 120 mg/L IPTG for 5 h. Cells were harvested and washed with PBS before freezing in liquid nitrogen. Thawed cells were resuspended in 20 mL lysis

buffer (25 mM Hepes, 800 mM KCl, 10% glycerol, 4% Triton X-100, 2 mM EDTA, 1 mM PMSF, complete protease inhibitor cocktail (Roche), 2 mM β-mercaptoethanol pH = 6.8-7.0), and sonicated to break up DNA. Cell debris were spun down at 13,000 rpm for 30 min, and resulting supernatant was added to 500 μL packed beads (glutathione, Fisher; Ni-NTA, Invitrogen) and incubated for 2 h at 4 °C. Beads were washed in batch with 30 volumes lysis buffer followed by 40 volumes wash buffer 1 (25 mM Hepes, 500 mM KCl, 10% glycerol, 0.5% Triton X-100, 1 mM EDTA, complete protease inhibitor cocktail (Roche), β-mercaptoethanol pH = 6.8-7.0) and another 40 volumes of wash buffer 2 (25 mM Hepes, 500 mM KCl, 10% Glycerol, 0.1% NP-40, 1 mM EDTA, complete protease inhibitor cocktail (Roche), β-mercaptoethanol pH = 6.8-7.0). Elution (25 mM Hepes, 50 mM KCl, 10% glycerol, 0.1% NP-40, 1 mM EDTA, 50 mM glutathione, complete protease inhibitor cocktail (Roche), 2 mM β-mercaptoethanol pH = 8.2-8.5) was operated on a column in 1 mL fractions, and run on an acrylamide gel to determine relevant fractions.

Binding assay—Ten microliters of packed glutathione agarose beads/tube were washed twice with binding buffer (10 mM Tris pH 7.4, 150 mM NaCl, 0.5 mM EDTA, 0.5% NP-40). Five micrograms of 6xHis-syntaxin-5 ΔNT and 5 μg GST-TEV-GPP130 proteins were added in a total volume of 200 μL and incubated for 2 h at 4 °C. Beads were washed 3x1 mL in binding buffer, and then resuspended in reducing sample buffer for analysis on acrylamide gels with Coomassie Blue.

Cell based assay—A GPP130 knockout cell line was transfected using JetPEI (VWR) according to the supplier's protocol with GPP130-GFP constructs (wild-type and KR-mutant), and passed on to coverslips after 6 h for assay the following day. Cells were treated with drugs (untreated, 100 μg/mL cycloheximide, cycloheximide+10 mM monensin) (Sigma) for 1 h. The monensin wells were then washed 5x1 mL with media, and all were incubated for a further 3 h in the presence of cycloheximide. Cells were fixed in 3% paraformaldehyde for 15 min, washed 3x1 mL with PBS followed by a 30 min block in block B (PBS with 5% FBS, 200 mM glycine and 0.5% Triton X-100). They were then incubated with rabbit anti-giantin antibody for 30 min in block, washed 3x1 mL with PBS, and further incubated with goat anti-rabbit, Alexa-568 secondary antibody (Invitrogen) in block buffer for another 30 min. Coverslips were mounted on slides after a final wash with 3x1 mL PBS. Cells were imaged and counted into bins of Golgi only, Golgi+endosomes, or endosomes only.

Click chemistry labeling

Copper-free click reactions were essentially performed as per manufacturer's recommendations. Briefly, HeLa cells were treated with 25 μM of the clickable Retro-the Retro-2.1 (compound **2)** for 30 min at 37 °C. The copper free click-reaction was performed on cells with DIBO-probes (Invitrogen, Click-iT reagents, 10 μM, compound **3** and **4**) for 1 h at room temperature and covered from light. For immunofluorescence microscopy, cells were fixed for 10 min at room temperature with 4% paraformaldehyde. For silver gel, western blot, and mass spectrometry analysis, the cells were lysed for 30 min at 4 °C with TNE buffer containing 1% NP-40 and complete protease inhibitor cocktail (Roche), followed by immunoprecipitation (see below).

Immunoprecipitation

Interacting partners of Syn5 were identified in a HeLa cell line stably expressing a Syn5-GFP fusion protein. Sec16A interacting proteins were identified in HeLa cells transiently transfected with GFP-Sec16A (harvested 20 h post transfection), treated with 25 μM Retro-2.1 or 0.05% DMSO for 30 mins. Cells were lysed for 30 min on ice in TNE buffer (100 mM PBS, 150 mM NaCl, 1% NP-40, complete protease inhibitor cocktail (Roche); for GFP-Sec16A 0.05% NP-40) and centrifuged for 10 min at 12,000xg, 4 °C. NeutrAvidin® beads (from Thermo Scientific; for clickable Retro-2.1 pull-down) or GFP-trap beads (25 μL per sample) (from Chromotek; for Syn5-GFP pull-down) were equilibrated in lysis buffer. Beads were collected by centrifugation (5 min, 500xg), or on strong magnets, following the manufacturer's instructions. The respective beads were incubated over night at 4 °C with 1.8 mg/mL cell lysates on an end-over-end rotation device. Competition with Retro-2.1 was performed to determine the specificity of binding partners (for pull-down experiments with clickable Retro-2.1 (compound **2**)), or to detect interactions that are sensitive to this compound (Syn5-GFP pull-down experiments). Vehicle alone (DMSO) was used as control. After three washing steps, samples were prepared for either mass spectrometry analysis (see proteomics and mass spectrometry analysis section), or for western blot analysis. Interacting proteins were eluted for 10 min at 95 °C in Laemmli buffer (0.1% 2-mercaptoethanol, 0.5 ‰ bromophenol blue, 10% glycerol, 2% SDS, 63 mM Tris-HCl, pH 6.8). The samples were analyzed by SDS-PAGE and either silver stained, western blotted for the indicated proteins, or digested for mass spectrometry analysis.

Retro-2 interaction with purified $Sec16A_{1266\text{-}1678}$/Sec13 was done on magnetic streptavidin beads purchased from Invitrogen. After equilibration, beads were saturated with a 33-fold excess of Retro-2.1-biotin (compound **5**) for 2 h at room temperature on a rotor. Twenty μg purified protein was incubated with loaded beads at 4 °C overnight on a rotor. After washing, the bound fraction was eluted in Laemmli buffer. The samples were analyzed by western blotting for the His-tag on the $Sec16A_{1266\text{-}1678}$ protein fragment.

Proteomics and liquid chromatography coupled to mass spectrometry analysis (LC-MS/MS)

Sample preparation—GFP-Syn5 samples were prepared as described above. For eluted Retro-2.1-biotin samples, these were run for 30 min at 30 mA on 10% Bis-Tris NuPAGE gels until the samples had just entered the gel, as a sample clean-up step. Samples were then split in half by excising the bands in 2 slices. Subsequently, gel slices were washed, and proteins were reduced with 10 mM DTT before alkylation with 55 mM iodoacetamide. After washing and shrinking the gel pieces with 100% MeCN, in-gel digestion was performed overnight at 30 °C using trypsin/LysC (Promega) in 25 mM NH_4HCO_3. Peptides were then extracted using 60/35/5 MeCN/H_2O/HCOOH, and vacuum-concentrated to dryness. Proteins interacting with GFP-Syn5 on the magnetic beads were washed twice with 100 μL of 25 mM NH_4HCO_3. On-bead digestion was performed for 1 h with 0.2 μg of trypsine/LysC (Promega) in 50 μL of 25 mM NH_4HCO_3. Samples were then loaded onto homemade C18 StageTips for desalting. Peptides were eluted using 40/60 MeCN/H_2O + 0.1% formic acid, and vacuum-concentrated to dryness. Peptides were resuspended in 2% MeCN, 0.3% TFA, separated, and analyzed by nanoLC-MS/MS using an UltiMate 3000 RSLCnano system

(Thermo Scientific) coupled to an Orbitrap Fusion (Q-OT-qIT, Thermo Fisher Scientific) mass spectrometer.

LTQ Orbitrap XL analysis (clickable Retro-2.1 and GFP-Syn5)—Peptides were loaded onto a C18-reversed phase precolumn (300 μm inner diameter × 5 mm, Thermo Scientific), and peptide separation was then performed over a linear gradient of 160 min from 0% to 30% of solvent B (80% acetonitrile, 0.085% formic acid; solvent A: 2% acetonitrile, 0.1% formic acid; column: 75 μm inner diameter × 50 cm; C18 PepMapTM, 3 μm, 100 Å, Thermo Scientific). The mass spectrometer was set to acquire a single MS in the Orbitrap analyzer with a resolution set to 60,000, followed by up to five data dependent scans (exclusion repeat count of 1, repeat duration of 30 s, exclusion duration of 180 s, and lock-mass option was enabled) with the ions from each full scan, CID fragmented, and analyzed in the linear ion trap.

Orbitrap Fusion analysis (GFP-Sec16A)—Peptides were first trapped on a C18 column (75 μm inner diameter × 2 cm; nanoViper Acclaim PepMapTM 100, Thermo Scientific) with buffer A (2/98 MeCN/H_2O in 0.1% formic acid) at a flow rate of 4 μL/min over 4 min. Separation was then performed on a 50 cm x 75 μm C18 column (nanoViper Acclaim PepMapTM RSLC, 2 μm, 100 Å, Thermo Scientific) regulated to a temperature of 55 °C with a linear gradient of 5% to 30% of buffer B (100% MeCN in 0.1% formic acid) at a flow rate of 300 nL/min over 100 min. Full-scan MS was acquired in the Orbitrap analyzer with a resolution set to 120,000. Ions from each full scan were HCD fragmented, and analyzed in the linear ion trap. The resulting spectra were then analyzed with Sequest™ through Proteome Discoverer (versions 2.1 or 2.2, Thermo Scientific) by using the SwissProt Homo sapiens Protein Database (022017 and 012018). Carbamidomethyle cysteine (for in-gel digestion only), oxidation of methionine, and N-terminal acetylation were set as variable modifications. Specificity of trypsin digestion was set, 2 missed cleavage sites was allowed for, and mass tolerances in MS and MS/MS was set to 10 ppm and 0.6 Da, respectively. The resulting files were further processed by using myProMS (v 3.5, Ref.[53]). The Sequest target and decoy search result were validated with Percolator at 1% false discovery rate (FDR).

GFP-Sec16A and GFP-Syn5—Label free quantification from bead samples was performed by peptide Extracted Ion Chromatograms (XICs) computed with MassChroQ version 2 (Ref.[54]). For protein quantification, XICs from proteotypic peptides shared between compared conditions (TopN matching) with missed cleavages were used. Median & Scale normalization was applied on the total signal to correct the XICs for each biological replicate. To estimate the significance of the change in protein abundance, a two-tailed t-test was performed using a linear model (adjusted on peptides and replicates), and p-values were adjusted with a Benjamini–Hochberg FDR procedure with a control threshold set to 0.05.

Result lists have been included as Supplementary Datasets 1-3.

The mass spectrometry proteomics data have been deposited to the ProteomeXchange Consortium via the PRIDE partner repository[55] with the dataset identifier project accession PXD015642.

Shiga toxin trafficking

HeLa cells, either DMSO or Retro-2 treated, were incubated for 30 min on ice with 2 μM (0.85 μg/mL) of STxB-Cy3. After the removal of unbound STxB-Cy3, its trafficking was initiated and followed for 45 min at 37 °C in the presence of DMSO or Retro-2. Cells were fixed for 10 min at RT with 4% paraformaldehyde (PFA), permeabilized with 0.25 mg/mL saponin, and immune-labeled with the indicated antibodies.

Proximity ligation assay (PLA)

For the PLA assay[56], HeLa cells were incubated for 30 min at 37 °C with 25 μM Retro-2 in complete medium, fixed for 10 min at room temperature with 4% PFA, permeabilized with 0.25 mg/mL saponin, and immunolabeled for 30 min for Syn5 and GS28 or GS27, after which PLA was performed according to the manufacturer's instructions (Duolink In Situ Orange Starter kit Mouse/Rabbit; Sigma-Aldrich). For quantification, at least 25 cells per experiment (n=2) were analyzed in each condition.

Confocal imaging

The majority of images were acquired on an inverted Eclipse Ti-E (Nikon) microscope equipped with a spinning disk CSU-X1 (Yokogawa) module, a x60 CFI Plan Apo VC oil objective, and Metamorph software by Gataca Systems. Z-stacks were acquired at a step size of 0.5 μm. Pixel size was 0.267 μm.

Images in Figures 1e, 3a, 3c, 4a,c, were imaged on an inverted Nikon Ti-E microscope with motorized XY stage (for Ti-E/Ni-E) fitted with a confocal A1R system, using a 60x oil immersion objective. Nikon NIS software, version 3.2.6 (Minato, Tokyo, Japan) was used for image acquisition.

Image Quantification

Fiji ImageJ software (National Institutes of Health, Bethesda, USA)[57] was used for image processing and quantification.

Fluorescence in the Golgi: A Golgi ROI was defined by giantin or TGN46 fluorescence. The Golgi channel was thresholded, ROIs defined, and then added to ROI manager using the Analyze Particles tool. Threshold values were maintained throughout each experimental set. Golgi ROI was superimposed onto the channel of interest (STxB, Syn5, GPP130). Fluorescence in Golgi ROI was measured by recording "RawIntDen" (the sum of the values of the pixels in the selection, from measurements selection in Fiji), and normalized to RawIntDen of the whole cell. A single mid-z stack image was analyzed per cell.

Colocalization with endosomes: An object-based 3D co-localization method was implemented in Imaris Bitplane software using customized analysis with Matlab (Imaris XT). First, individual objects (endosomes) were segmented in both channels and represented as points through coordinates of their centers of mass. Then, the distance of each point of the first population (Channel 1) to nearest-neighbor in the second population (Channel 2) was estimated. Spots in the first population were considered co-localized when the distance was smaller or equal to 0.5 μm.

GraphPad Prism 8 was used to produce graphs and perform statistics.

Retention using selective hooks (RUSH)

The RUSH system was adopted as previously published[58]. Briefly, the Syn5-SBP-eGFP gene was cloned into a RUSH construct with the AscI and XbaI restriction sites. After overnight transfection, cells were treated with Retro-2 or DMSO, as described above. Trafficking was initiated with 40 μM biotin in complete medium. Cells were kept 20 min at 37 °C, before being fixed for 10 min at room temperature with PFA. Immunolabeling was performed as indicated.

FRAP protocol

HeLa cells were mock transfected, or transfected with siRNA against Sar1A/B (siGENOME, Dharmacon) to a final concentration of 100 nM with Lipofectamine (Invitrogen), according to manufacturer's instructions. 15 h later, all cells were transfected with GFP-Sec23A[59], and seeded in glass bottomed dishes (FD35-100, FluoroDish, World Precision Instruments). Cells were treated for 45 min with 25 μM Retro-2 or 0.05% DMSO, and imaged at 37 °C for a maximum of 1 h in a humidified atmosphere with 5% CO_2. Experiments were performed on a Ti-E inverted spinning disk confocal Nikon microscope with ILas2 FRAP module (Errol and Roper, France), using a 100x 1.4 NA CFI Plan Apo VC oil immersion objective and CCD camera (CoolSnap HQ2 Photometrics, USA) with a pixel size of 64.5 nm. Acquisitions were performed in streaming mode using Metamorph 7.7.6 software (Molecular Devices, France). Photobleaching of single ER exit sites per cell was performed with a conserved region of interest (0.8 μm) to avoid non-specific bleaching. Bleaching laser was set to 85% with 50 iterations, to obtain about 60% of the pre-bleach fluorescence. After photobleaching, images were acquired every 750 ms for 5 s, followed by every 2 s for 10 s, and finally every 10 s for 20 s using 20% laser intensity. Image analysis was performed in ImageJ. Data were exported to Prism and statistics performed as described below.

Intoxication Assay

SLT1 intoxication was performed on specific or scrambled siRNA-transfected HeLa cells[23]. Briefly, 20,000 HeLa cells per well were seeded into flat-bottomed 96-well optical plates (Nunc) and grown overnight at 37 °C. After pretreatment with Retro-2 or DMSO, cells were incubated for 1 h at 37 °C with increasing doses of SLT1 from 0,005 to 100 ng/mL. After washes with PBS, 1 μCi [35S]-methionine (Perkin Elmer) was added for 60 min at 37 °C to each well. Radiolabeled proteins were precipitated by washing cells three times at 4 °C with 5% trichloroacetic acid (TCA). Before liquid scintillation measurements, TCA was removed by three washes with PBS. Normalized duplets were used to determine the mean percentage of protein biosynthesis. The Prism software, version 7 (GraphPad, CA, USA) was used to fit and calculate the 50% effective toxin concentration (EC_{50}) from sigmoidal dose response fitting. Protection factors are shown as EC_{50}drug/EC_{50}control and EC_{50}siRNA/EC_{50}control.

Western blot analysis

Cells on a thermo-shaker were lysed for 10 min at 95 °C in Laemmli buffer. Samples were size separated via SDS-PAGE. Proteins were transferred onto nitrocellulose membranes with Pierce™ Power blotter (Thermo Fisher Scientific, Waltham, MA, USA). The following antibody dilutions were used: Syn5 (1:1000), GS27 (1:1000), GS28 (1:1000), and GFP (1:5000). Corresponding HRP-coupled secondary antibodies (1:5000, Jackson ImmunoResearch Laboratories, West Grove, PA, USA) were used. Protein bands were visualized with SuperSignal (Thermo Scientific), and analyzed on a Fusion S western blot imager (Vilber Lourmat, Marne-la-Vallée, France). Densitometry analysis of the gels was carried out using ImageJ software from the NIH.

FortéBio Octet system assay

The FortéBio Octet® Red96e system (FortéBio Inc., USA) was used to determine the interactions between the biotinylated Retro-2.1 probe (compound **15**) and the $Sec16A_{1266\text{-}1678}$/Sec13 protein complex. Experiments were performed at 20 °C using streptavidin biosensors. The Octet assay protocol was performed as follows: Baseline 1 (PBS buffer) for 120 s; loading (0 or 250 nM biotinylated Retro-2.1 probe (compound **15**) in PBS) for 120 s; baseline 2 for 120 s in blocking buffer (PBS with 1% BSA, 0.1% Tween-20, 20 μg/mL biotin); baseline 3 in kinetics buffer (PBS with 0.1% BSA, 0.02% Tween-20); association with various concentrations of $Sec16A_{1266\text{-}1678}$/Sec13 for 600 s; dissociation for 2,000 s in kinetics buffer. The protein sample concentration was ranging from 0.5 to 3 μM. Kinetic constants were calculated from the raw data using the data analysis software (version 10.0, FortéBio) with a curve fit 1:1 model performed using global fit ($R^2 = 0.984$).

Statistics

All data are presented as mean ± SD. Unpaired Student's t tests were used to determine the statistical significance of possible differences between two data sets. One-way ANOVA was used to perform analyses between more than 2 samples, with Dunnett's multiple comparison tests to compare control to test conditions. A value of $P \leq 0.05$ was considered as significant. For FRAP experiments, one-way ANOVA (*$P<0.033$) with Dunnett's multiple comparisons test was used (ns $P>0.123$, ** $P<0.002$). GraphPad Prism Software 8 (GraphPad, San Diego, CA) was used to illustrate the graphs and perform the analysis.

Supplementary Material

Refer to Web version on PubMed Central for supplementary material.

Acknowledgements

We thank Raphaël Rodriguez (cell imaging of Retro-2.1 and target identification), Gaëlle Boncompain (RUSH), Christine Viaris De Lesegno (PLA), Rosine Onclercq-Delic, Sophie Bombard (intoxication assay), Clémence Brewee and Bastien Sancerne (recombinant protein production and cytotoxicity assays), David Buisson (purification of compound 15), and Egor Chirkin (synthesis of new batch of chemicals) for help with the indicated experiments. We thank Valentin Sabatet from the LSMP for myProMS assistance. We acknowledge support by grants from the Agence Nationale pour la Recherche (ANR-11-BSV2-0018 and ANR-14-CE16-0004-03 to LJ, JB, JCC and DG; ANR-19-CE13-0001-01 to LJ), Human Frontier Science Program (RGP0029-2014 to LJ), European Research Council (advanced grant 340485 to LJ), the Swedish Research Council (K2015-99X-22877-01-6 to LJ, JCC and DG), the Joint ministerial program of R&D against CBRNE risks (to DG, JB, JCC and LJ), CEA (to DG,

JB and JCC), Ile de France Region DIM Malinf initiative (grant 140101 to DG, JB and LJ), Région Ile-de-France (DL), and Fondation pour la Recherche Médicale (DL). The Gillet and Cintrat teams are members of LabEx LERMIT (ANR-10-LABX-33), and the Johannes team of Labex CelTisPhyBio (11-LBX-0038) and Idex Paris Sciences et Lettres (ANR-10-IDEX-0001-02 PSL). We would also like to acknowledge the Cell and Tissue Imaging (PICT-IBiSA) and Nikon Imaging Centre, Institut Curie, member of the French National Research Infrastructure France-BioImaging (ANR10-INBS-04).

References

1. Johannes L, Römer W. Shiga toxins - from cell biology to biomedical applications. Nat Rev Microbiol. 2010; 8:105–116. [PubMed: 20023663]
2. Tarr PI, Gordon CA, Chandler WL. Shiga-toxin-producing Escherichia coli and haemolytic uraemic syndrome. Lancet. 2005; 365:1073–1086. [PubMed: 15781103]
3. Endo Y, et al. Site of action of a Vero toxin (VT2) from Escherichia coli O157:H7 and of Shiga toxin on eukaryotic ribosomes. RNA N-glycosidase activity of the toxins. Eur J Biochem. 1988; 171:45–50. [PubMed: 3276522]
4. Fraser ME, Chernaia MM, Kozlov YV, James MN. Crystal structure of the holotoxin from Shigella dysenteriae at 2.5 A resolution. Nat Struct Biol. 1994; 1:59–64. [PubMed: 7656009]
5. Ling H, et al. Structure of Shiga-like toxin I B-pentamer complexed with an analogue of its receptor Gb3. Biochemistry. 1998; 37:1777–1788. [PubMed: 9485303]
6. Sandvig K, Olsnes S, Brown JE, Petersen OW, van Deurs B. Endocytosis from coated pits of Shiga toxin: a glycolipid-binding protein from Shigella dysenteriae 1. J Cell Biol. 1989; 108:1331–1343. [PubMed: 2564398]
7. Römer W, et al. Shiga toxin induces tubular membrane invaginations for its uptake into cells. Nature. 2007; 450:670–675. [PubMed: 18046403]
8. Mallard F, et al. Early/recycling endosomes-to-TGN transport involves two SNARE complexes and a Rab6 isoform. J Cell Biol. 2002; 156:653–664. [PubMed: 11839770]
9. Sandvig K, et al. Retrograde transport of endocytosed Shiga toxin to the endoplasmic reticulum. Nature. 1992; 358:510–512. [PubMed: 1641040]
10. Spooner RA, Lord JM. How ricin and Shiga toxin reach the cytosol of target cells: retrotranslocation from the endoplasmic reticulum. Curr Top Microbiol Immunol. 2012; 357:19–40. [PubMed: 21761287]
11. Johannes L, Popoff V. Tracing the retrograde route in protein trafficking. Cell. 2008; 135:1175–1187. [PubMed: 19109890]
12. Sandvig K, Skotland T, van Deurs B, Klokk TI. Retrograde transport of protein toxins through the Golgi apparatus. Histochem Cell Biol. 2013; 140:317–326. [PubMed: 23765164]
13. Bujny MV, Popoff V, Johannes L, Cullen PJ. The retromer component, sorting nexin-1, is required for efficient early endosome-to-trans Golgi network retrograde transport of Shiga toxin. J Cell Sci. 2007; 120:2010–2021. [PubMed: 17550970]
14. Popoff V, et al. The retromer complex and clathrin define a post-early endosomal retrograde exit site. J Cell Sci. 2007; 120:2022–2031. [PubMed: 17550971]
15. Utskarpen A, Slagsvold HH, Dyve AB, Skanland SS, Sandvig K. SNX1 and SNX2 mediate retrograde transport of Shiga toxin. Biochem Biophys Res Commun. 2007; 358:566–570. [PubMed: 17498660]
16. Mukhopadhyay S, Linstedt AD. Manganese blocks intracellular trafficking of Shiga toxin and protects against Shiga toxicosis. Science. 2012; 335:332–335. [PubMed: 22267811]
17. Mukhopadhyay S, Redler B, Linstedt AD. Shiga toxin binding site for host cell receptor GPP130 reveals unexpected divergence in toxin trafficking mechanisms. Mol Biol Cell. 2013; 24:2311–2318. [PubMed: 23761068]
18. Tai G, et al. Participation of syntaxin 5/Ykt6/GS28/GS15 SNARE complex in transport from the early/recycling endosome to the TGN. Mol Biol Cell. 2004; 15:4011–4022. [PubMed: 15215310]
19. Hui N, et al. An isoform of the Golgi t-SNARE, syntaxin 5, with an endoplasmic reticulum retrieval signal. Mol Biol Cell. 1997; 8:1777–1787. [PubMed: 9307973]

20. Mancias JD, Goldberg J. Structural basis of cargo membrane protein discrimination by the human COPII coat machinery. Embo J. 2008; 27:2918–2928. [PubMed: 18843296]
21. Gillet, D; Barbier, J; Johannes, L; Cintrat, J-C; Noël, R. New compounds having a protective activity against toxins with intracellular activity. Patent WO2014060586A1. 2012.
22. Mukhopadhyay S, Linstedt AD. Retrograde trafficking of AB(5) toxins: mechanisms to therapeutics. J Mol Med (Berl). 2013; 91:1131–1141. [PubMed: 23665994]
23. Stechmann B, et al. Inhibition of retrograde transport protects mice from lethal ricin challenges. Cell. 2010; 141:231–242. [PubMed: 20403321]
24. Secher T, et al. Retrograde trafficking inhibitors of Shiga toxins reduces morbidity and mortality of mice Infected with enterohemorrhagic Escherichia coli (STEC). Antimicrob Agents Chemother. 2015; 59:5010–5013. [PubMed: 25987610]
25. Canton J, Kima PE. Targeting host syntaxin-5 preferentially blocks Leishmania parasitophorous vacuole development in infected cells and limits experimental Leishmania infections. Am J Pathol. 2012; 181:1348–1355. [PubMed: 22885104]
26. Gupta N, et al. Inhibitors of retrograde trafficking active against ricin and Shiga toxins also protect cells from several viruses, Leishmania and Chlamydiales. Chem Biol Interact. 2017; 267:96–103. [PubMed: 27712998]
27. Carney DW, et al. Structural optimization of a retrograde trafficking inhibitor that protects cells from infections by human polyoma- and papillomaviruses. Bioorg Med Chem. 2014; 22:4836–4847. [PubMed: 25087050]
28. Dai W, et al. Antiviral effects of Retro-2(cycl) and Retro-2.1 against Enterovirus 71 in vitro and in vivo. Antiviral Res. 2017; 144:311–321. [PubMed: 28688753]
29. Dai WW, et al. Antiviral Effect of Retro-2.1 against Herpes Simplex Virus Type 2 In Vitro. J Microbiol Biotechnol. 2018
30. Cruz L, et al. Potent Inhibition of Human Cytomegalovirus by Modulation of Cellular SNARE Syntaxin 5. J Virol. 2017; 91
31. Shtanko O, et al. Retro-2 and its dihydroquinazolinone derivatives inhibit filovirus infection. Antiviral Res. 2018; 149:154–163. [PubMed: 29175127]
32. Harrison K, et al. Vaccinia Virus Uses Retromer-Independent Cellular Retrograde Transport Pathways To Facilitate the Wrapping of Intracellular Mature Virions during Virus Morphogenesis. J Virol. 2016; 90:10120–10132. [PubMed: 27581988]
33. Sivan G, Weisberg AS, Americo JL, Moss B. Retrograde Transport from Early Endosomes to the trans-Golgi Network Enables Membrane Wrapping and Egress of Vaccinia Virus Virions. J Virol. 2016; 90:8891–8905. [PubMed: 27466413]
34. Noel R, et al. N-Methyldihydroquinazolinone Derivatives of Retro-2 with Enhanced Efficacy against Shiga Toxin. J Med Chem. 2013; 56:3404–3413. [PubMed: 23517565]
35. Whittle JR, Schwartz TU. Structure of the Sec13-Sec16 edge element, a template for assembly of the COPII vesicle coat. J Cell Biol. 2010; 190:347–361. [PubMed: 20696705]
36. Wälchli S, et al. The Mitogen-activated Protein Kinase p38 Links Shiga Toxin-dependent Signaling and Trafficking. Mol Biol Cell. 2008; 19:95–104. [PubMed: 17959827]
37. Hughes H, Stephens DJ. Assembly, organization, and function of the COPII coat. Histochem Cell Biol. 2008; 129:129–151. [PubMed: 18060556]
38. Xu Y, Martin S, James DE, Hong W. GS15 Forms a SNARE Complex with Syntaxin 5, GS28, and Ykt6 and Is Implicated in Traffic in the Early Cisternae of the Golgi Apparatus. Mol Biol Cell. 2002; 13:3493–3507. [PubMed: 12388752]
39. Chen YA, Scheller RH. SNARE-mediated membrane fusion. Nat Rev Mol Cell Biol. 2001; 2:98–106. [PubMed: 11252968]
40. Hong W. SNAREs and traffic. Biochim Biophys Acta. 2005; 1744:493–517. [PubMed: 16038056]
41. Amessou M, et al. Syntaxin 16 and syntaxin 5 control retrograde transport of several exogenous and endogenous cargo proteins. J Cell Sci. 2007; 120:1457–1468. [PubMed: 17389686]
42. Puri S, Bachert C, Fimmel CJ, Linstedt AD. Cycling of early Golgi proteins via the cell surface and endosomes upon lumenal pH disruption. Traffic. 2002; 3:641–653. [PubMed: 12191016]

43. Natarajan R, Linstedt AD. A cycling cis-Golgi protein mediates endosome-to-Golgi traffic. Mol Biol Cell. 2004; 15:4798–4806. [PubMed: 15331763]
44. Linstedt AD, Mehta A, Suhan J, Reggio H, Hauri HP. Sequence and overexpression of GPP130/GIMPc: evidence for saturable pH-sensitive targeting of a type II early Golgi membrane protein. Mol Biol Cell. 1997; 8:1073–1087. [PubMed: 9201717]
45. Ledger PW, Uchida N, Tanzer ML. Immunocytochemical localization of procollagen and fibronectin in human fibroblasts: effects of the monovalent ionophore, monensin. J Cell Biol. 1980; 87:663–671. [PubMed: 7007394]
46. Mollenhauer HH, Morre DJ, Rowe LD. Alteration of intracellular traffic by monensin; mechanism, specificity and relationship to toxicity. Biochim Biophys Acta. 1990; 1031:225–246. [PubMed: 2160275]
47. Cañeque T, Muller S, Rodriguez R. Visualizing biologically active small molecules in cells using click chemistry. Nat Rev Chem.
48. Adolf F, Rhiel M, Reckmann I, Wieland FT. Sec24C/D-isoform-specific sorting of the preassembled ER-Golgi Q-SNARE complex. Mol Biol Cell. 2016; 27:2697–2707. [PubMed: 27413010]
49. Campbell JL, Schekman R. Selective packaging of cargo molecules into endoplasmic reticulum-derived COPII vesicles. Proc Natl Acad Sci USA. 1997; 94:837–842. [PubMed: 9023343]
50. Gupta N, et al. (S)-N-methyldihydroquinazolinones are the active enantiomers of Retro-2 derived compounds against toxins. ACS Med Chem Lett. 2014; 5:94–97. [PubMed: 24900779]
51. Mallard F, et al. Direct pathway from early/recycling endosomes to the Golgi apparatus revealed through the study of Shiga toxin B-fragment transport. J Cell Biol. 1998; 143:973–990. [PubMed: 9817755]
52. Jordan M, Schallhorn A, Wurm FM. Transfecting mammalian cells: optimization of critical parameters affecting calcium-phosphate precipitate formation. Nucleic Acids Res. 1996; 24:596–601. [PubMed: 8604299]
53. Poullet P, Carpentier S, Barillot E. myProMS, a web server for management and validation of mass spectrometry-based proteomic data. Proteomics. 2007; 7:2553–2556. [PubMed: 17610305]
54. Valot B, Langella O, Nano E, Zivy M. MassChroQ: a versatile tool for mass spectrometry quantification. Proteomics. 2011; 11:3572–3577. [PubMed: 21751374]
55. Vizcaino JA, et al. 2016 update of the PRIDE database and its related tools. Nucleic Acids Res. 2016; 44:11033. [PubMed: 27683222]
56. Soderberg O, et al. Direct observation of individual endogenous protein complexes in situ by proximity ligation. Nat Methods. 2006; 3:995–1000. [PubMed: 17072308]
57. Schindelin J, et al. Fiji: an open-source platform for biological-image analysis. Nat Methods. 2012; 9:676–682. [PubMed: 22743772]
58. Boncompain G, Perez F. Synchronizing protein transport in the secretory pathway. Curr Protoc Cell Biol. 2012; Chapter 15
59. Venditti R, et al. Sedlin controls the ER export of procollagen by regulating the Sar1 cycle. Science. 2012; 337:1668–1672. [PubMed: 23019651]

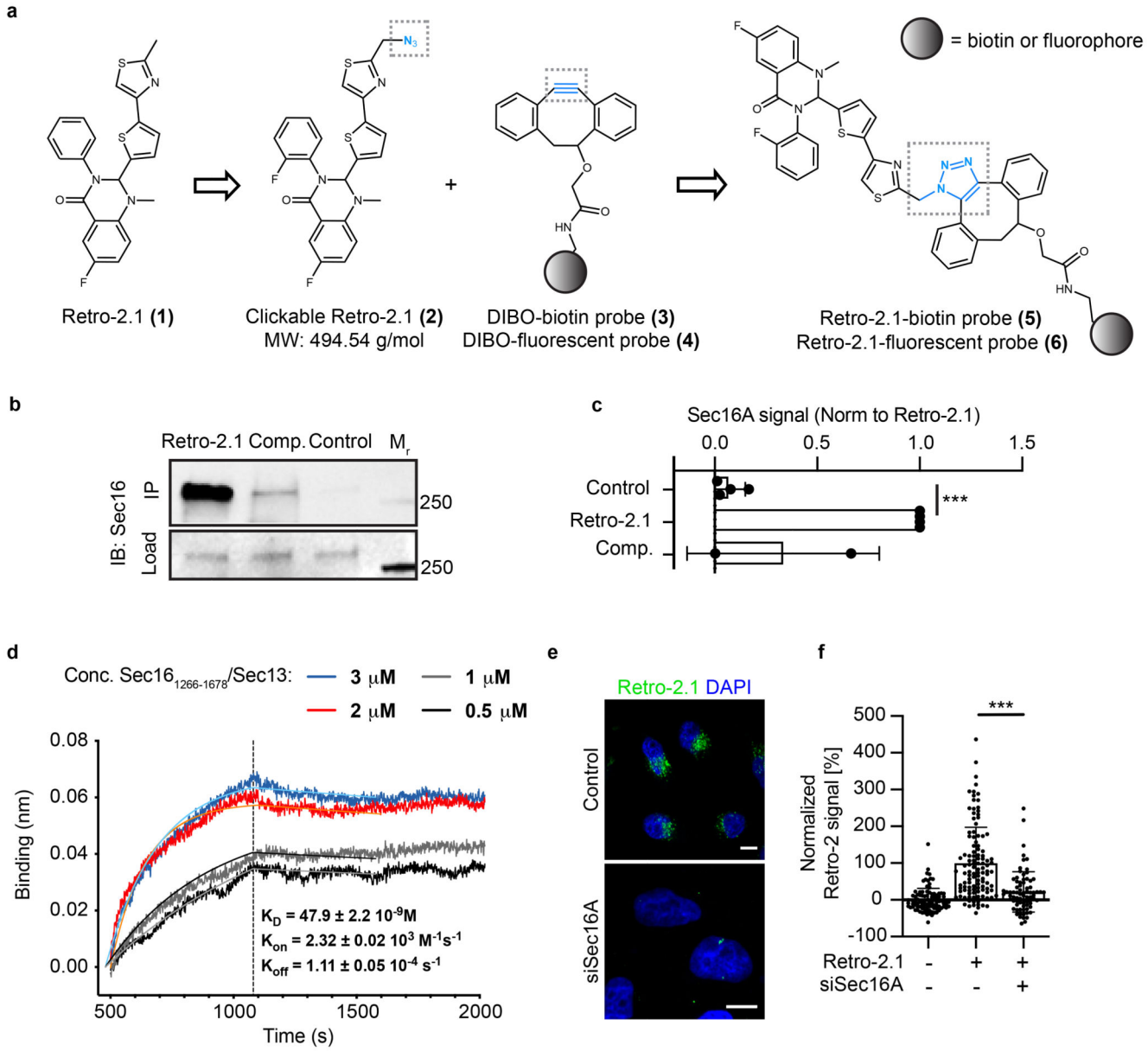

Figure 1. Retro-2 binds directly to Sec16A.

(**a**) Scheme of biorthogonal click chemistry adapted to Retro-2.1. The clickable Retro-2.1 (compound **2**), based on Retro-2.1 (compound **1**, Ref.[34, 50]) is coupled via the DIBO moiety to biotin (compound **3**), or a fluorophore (compound **4**). Blue/dashed boxes indicate reactive centers. (**b**) Anti-Sec16A western blot of a representative pull-down with the clickable Retro-2.1-probe (compound **5**). Load corresponds to the western blot of the input fraction. See Supplementary Fig. 7a for full gels. (**c**) Quantification of four (control and Retro-2.1) and two (competition, Comp.) independent experiments of clickable Retro-2.1 pull-down shown in (b). Bead control and competition conditions normalized to Retro-2.1 pull-down. Graph shows mean +/- SD, each point represents an individual experiment. Unpaired two-tailed t-test comparing Retro-2.1 to control, *** $P < 0.0001$. (**d**) Characterization of the

$Sec16A_{1266-1678}$/Sec13-Retro-2.1 interaction using bio-layer interferometry. Association and dissociation steps after subtraction of control curves (loading step without biotinylated Retro-2.1 probe) and analysis of binding kinetics of $Sec16A_{1266-1678}$/Sec13 to biotinylated Retro-2.1 (compound **5**). Graph is representative of 2 independent experiments. Data were acquired repeatedly from the same sample. (**e**) Confocal images of clickable Retro-2.1 reacted with an Alexa488 probe (compound **6**) on mock siRNA transfected (control) or Sec16A-depleted (siSec16A) cells. DNA was stained with DAPI. Scale bars = 10 μm. Image representative of 2 independent experiments. (**f**) Quantification of fluorescence intensity of clicked Retro-2.1 (compound **6)** in the indicated conditions. Quantification of 97 (negative control), 114 (Retro-2.1) and 77 (siSec16A) cells per condition from 2 independent experiments. Each point represents one cell. Negative control is fluorophore in the absence of clickable Retro-2.1 ("No Retro-2.1"). Graph shows mean +/- SD. Unpaired two-tailed t-test performed to compare Retro-2.1 treated and Retro-2.1+siSec16A conditions, *** $P < 0.0001$. See Supplementary Notes for numbered compound synthetic procedures.

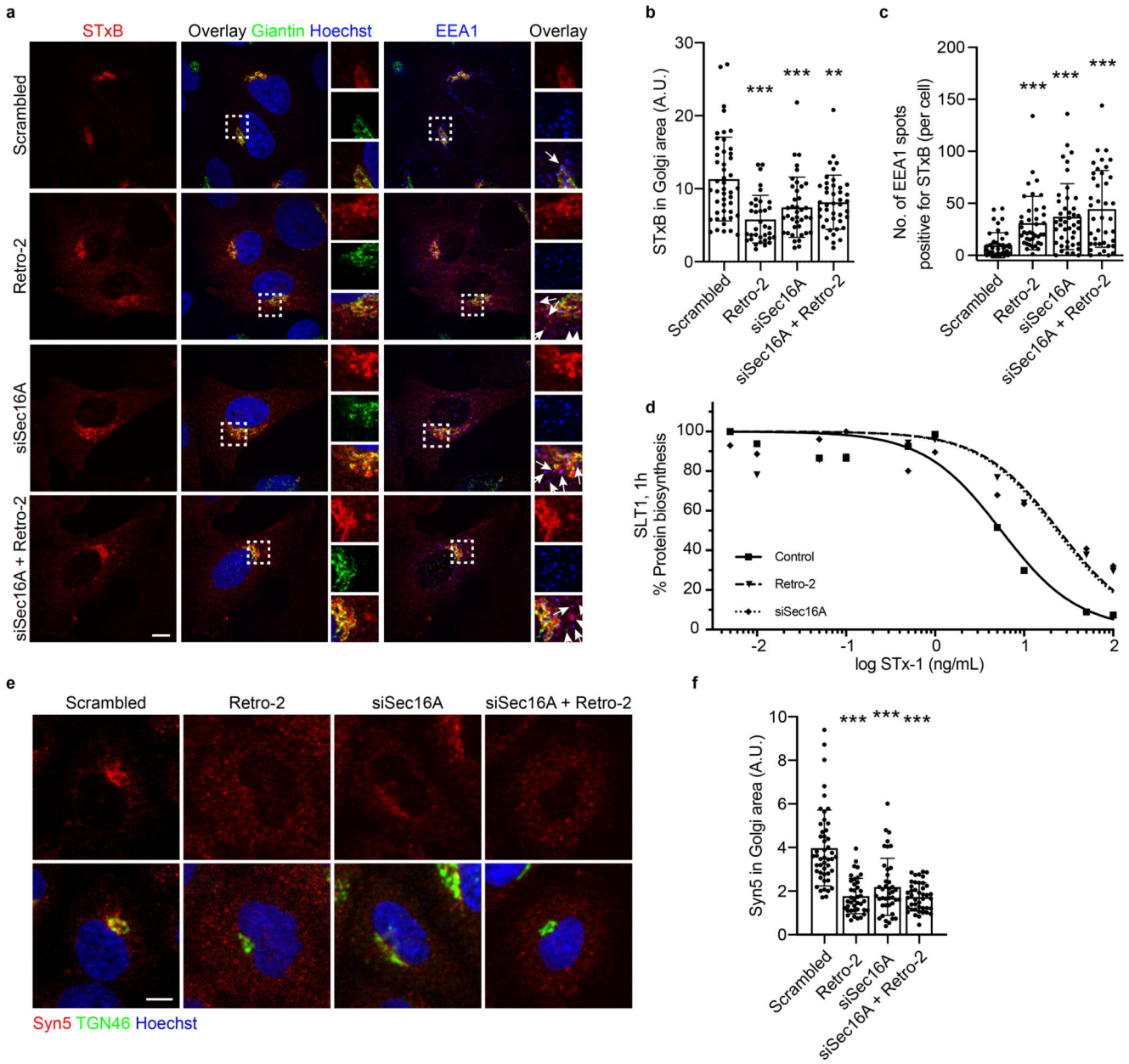

Figure 2. Depletion of Sec16A phenocopies Retro-2 effects.

(**a**) HeLa cells transfected with the indicated siRNAs, or treated for 30 min with 25 μM Retro-2, followed by incubation for 45 min at 37 °C with STxB-Cy3 (red). Cells were labeled for giantin (green, left panels) and EEA1 (blue, right panels). Nuclei were labeled with Hoechst (blue, left panels). Arrows indicate spots of STxB colocalized with EEA1, dotted lines indicate areas of zoomed panels. Scale bar = 10 μm. Representative images from 6 independent experiments (Giantin colocalisation) and 3 independent experiments (EEA1 colocalisation). (**b**) Quantification of STxB colocalization with Golgi area defined by giantin. Graph represents mean +/- SD for 46 (scrambled), 35 (Retro-2), 39 (siSec16A), 42 (Retro-2+siSec16A) cells from three independent experiments. Each point represents an

individual cell. One-way ANOVA was performed overall ($P < 0.0001$) with Dunnett's multiple comparison test to compare Scrambled to treated conditions (*** $P = 0.0002$, ** $P = 0.0021$). (**c**) Quantification of number of EEA1 spots positive for STxB. Graph represents mean +/- SD for a minimum of 40 cells from 3 independent experiments. One-way ANOVA was performed overall ($P < 0.0001$) with Dunnett's multiple comparison test to compare Scrambled to treated conditions (*** $P < 0.0001$). (**d**) Intoxication of HeLa cells with SLT1 in the indicated conditions. HeLa cells were transfected with either scrambled siRNA, or siRNAs against Sec16A. Where indicated, cells were incubated 30 min with 25 μM Retro-2 or vehicle (0.05% DMSO, "control"), before the addition of SLT1 for 1 h at the indicated concentrations. Medium was removed and replaced for 1 h with Ca^{2+} and Mg^{2+}-supplemented PBS containing [^{35}S]-methionine. Each data point represents the mean of a representative experiment, from 2 independent experiments. (**e**) HeLa cells were transfected with siSec16A and where indicated treated for 30 min with 25 μM Retro-2 or DMSO control. Cells were labeled for TGN46 (green) and Syn5 (red), and nuclei labeled with Hoechst (blue). Representative images from 3 independent experiments. (**f**) Quantification of Syn5 at Golgi area as defined by TGN46. Graph represents mean +/- SD for 48 (Scrambled), 39 (Retro-2), 41 (siSec16A), 43 (Retro-2 + siSec16A) cells from 3 independent experiments. Each point represents an individual cell. One-way ANOVA was performed overall ($P < 0.0001$) with Dunnett's multiple comparisons test to compare Scrambled to treated conditions (*** $P < 0.0001$).

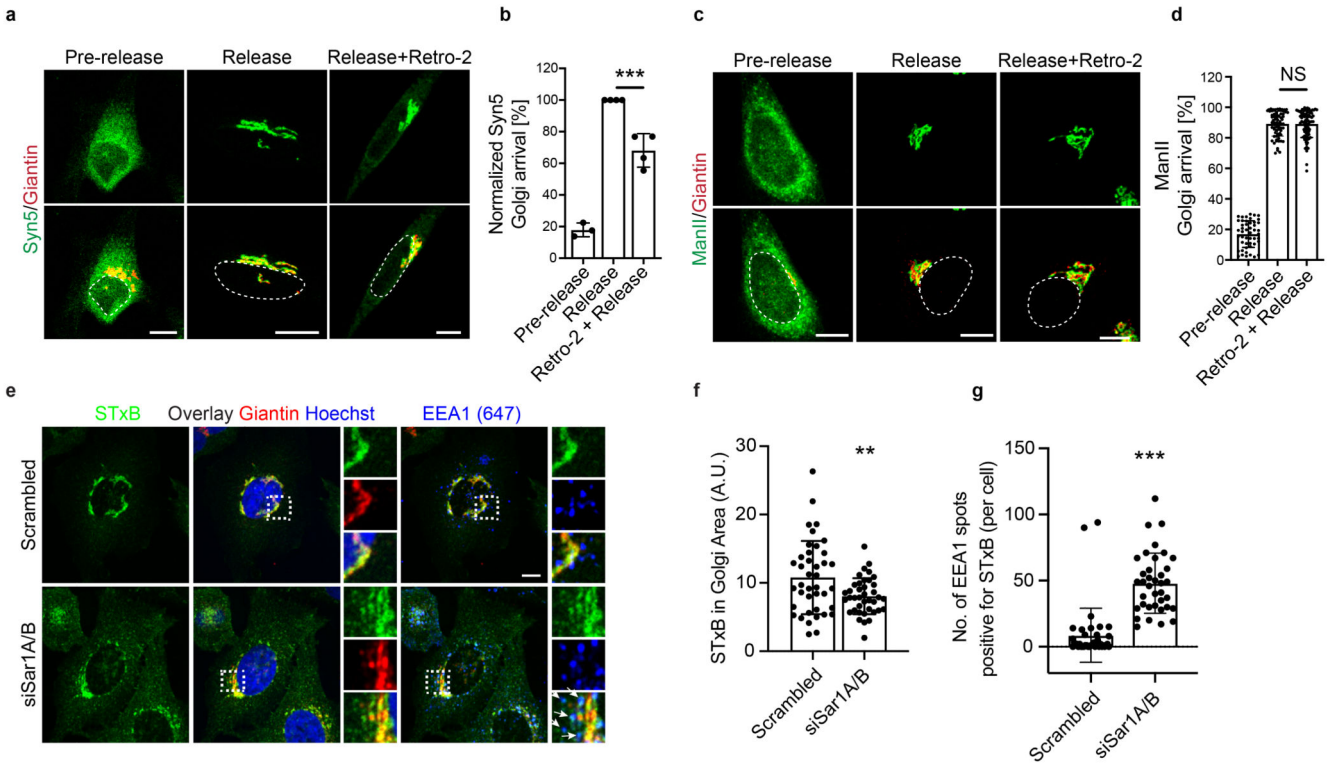

Figure 3. Retro-2 treatment slows the anterograde transport of Syn5.

(**a**) Confocal acquisitions of HeLa cells expressing Syn5-RUSH construct (green) or (**c**) ManII-RUSH construct (green) and labeled with anti-giantin (red). Cells were pre-treated for 60 min at 37 °C with 25 μM Retro-2, or 0.05% DMSO as control (pre-release). Trafficking was triggered by incubation with biotin for 20 min at 37 °C. Dashed lines indicate nuclei. Scale bars = 10 μm. Representative images from (a) 3 (pre-release) or 4 (Release and Retro-2 + release) independent experiments and (c) 2 independent experiments. (**b**) Quantification of Syn5-GFP intensity in the Golgi area, normalized to Release conditions. Graph shows mean +/- SD of 28 (Pre-release), 24 (Release), 56 (Release + Retro-2) cells per experiment from 3 (pre-release) or 4 (Release and Retro-2 + release) independent experiments, each point represents one experimental replicate. Unpaired two-tailed t-test performed between Release and Retro-2 + Release conditions, *** P = 0.001. (**d**) Quantification of ManII-GFP intensity in the Golgi area. Graph shows mean +/- SD for 48 (pre-release), 71 (release), 81 (release + Retro-2) cells per experiment from 2 independent experiments. Each point represents a single cell. Unpaired, two-tailed t-test, performed between Release and Retro-2 + Release conditions, NS = not significant, P = 0.936. (**e**) HeLa cells transfected with siSar1A/B, incubated for 45 min at 37 °C with STxB-Cy3 (green) and labeled with giantin (red) and EEA1 (blue in right panels). Nuclei were labeled with Hoechst (blue in left panels). Dotted lines indicate areas shown in zoom panels. Scale bar = 10 μm. Representative images from 3 independent experiments. (**f**) Quantification of STxB colocalization with Golgi area defined by giantin. Graph represents mean +/- SD for 40 (scrambled) and 39 (siSar1A/B) cells from 3 independent experiments. Each point represents one cell. Unpaired two-tailed t-test, ** P = 0.0055. (**g**) Quantification of number

of EEA1 spots positive for STxB. Graph represents mean +/- SD for 39 (scrambled) and 37 (siSar1A/B) cells from 3 independent experiments. Each point represents one cell. Unpaired two-tailed t-test, *** $P < 0.0001$.

Europe PMC Funders Author Manuscripts

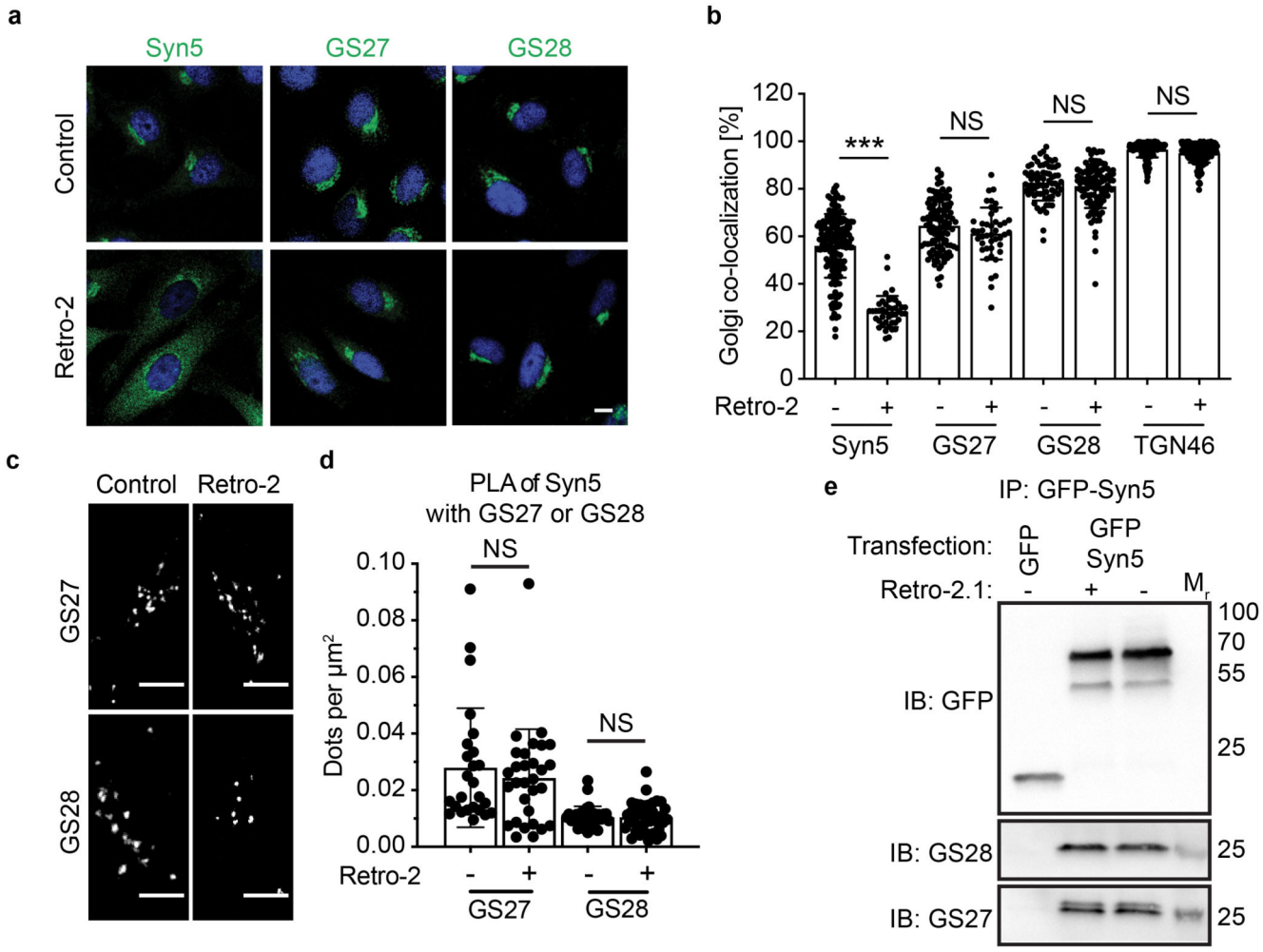

Figure 4. Syn5 SNARE complex formation is not affected by Retro-2.

(**a**) Representative confocal acquisitions of the cellular distribution of Syn5, GS27, and GS28 (green) in control (0.05% DMSO) or 25 µM Retro-2-treated cells, from 2 independent experiments. Nuclei marked by DAPI (blue). Scale bar = 10 µm. (**b**) Quantification of Syn5, GS27, or GS28 immunolabeling in the Golgi area, as defined by TGN46. Graph represents mean +/- SD for 180 (- Syn5), 43 (+ Syn5), 109 (- GS27), 43 (+ GS27), 71 (-GS28), 108 (+ GS28), 180 (- TGN46), 182 (+ TGN46) cells from 2 independent experiments. Each point represents one cell. One-way ANOVA was performed overall ($P < 0.0001$) with Sidak's multiple comparisons test comparing untreated and Retro-2 treated conditions for each protein; Syn5: *** $P < 0.0001$; GS27: NS $P = 0.1405$; GS28: NS $P = 0.7373$; TGN46: NS $P = 0.3446$. (**c**) Representative confocal acquisitions of proximity ligation assay (PLA) of Syn5 with either GS27 or GS28 on 0.05% DMSO (control) or 25 µM Retro-2-treated cells. Scale bars = 10 µm. Representative images from 2 independent experiments. (**d**) Quantification of fluorescent dots / μm^2 as shown in (c). Number of dots were normalized per μm^2. Graph shows mean +/- SD for 25 (- GS27), 30 (+ GS27), 31 (- GS28), 39 (+ GS28) cells from 2 independent experiments. Each point represents one cell. One-way ANOVA was performed overall (*** $P < 0.0001$) with Sidak's multiple comparisons test comparing

untreated and Retro-2 treated conditions for each protein; GS27: NS P = 0.5077; GS28: NS P = 0.9997. (**e**) Western blotting of a representative GFP-Syn5 pull-down from 2 independent experiments. GFP-transfected cells were used as controls. GFP-Syn5 cells were treated either with 0.05% DMSO (control), or with 25 μM Retro-2.1. Note that GS27 and GS28 were pulled-down with Syn5, irrespective of incubation with Retro-2.1. See Supplementary Fig. 7b for full gels.

Europe PMC Funders Author Manuscripts

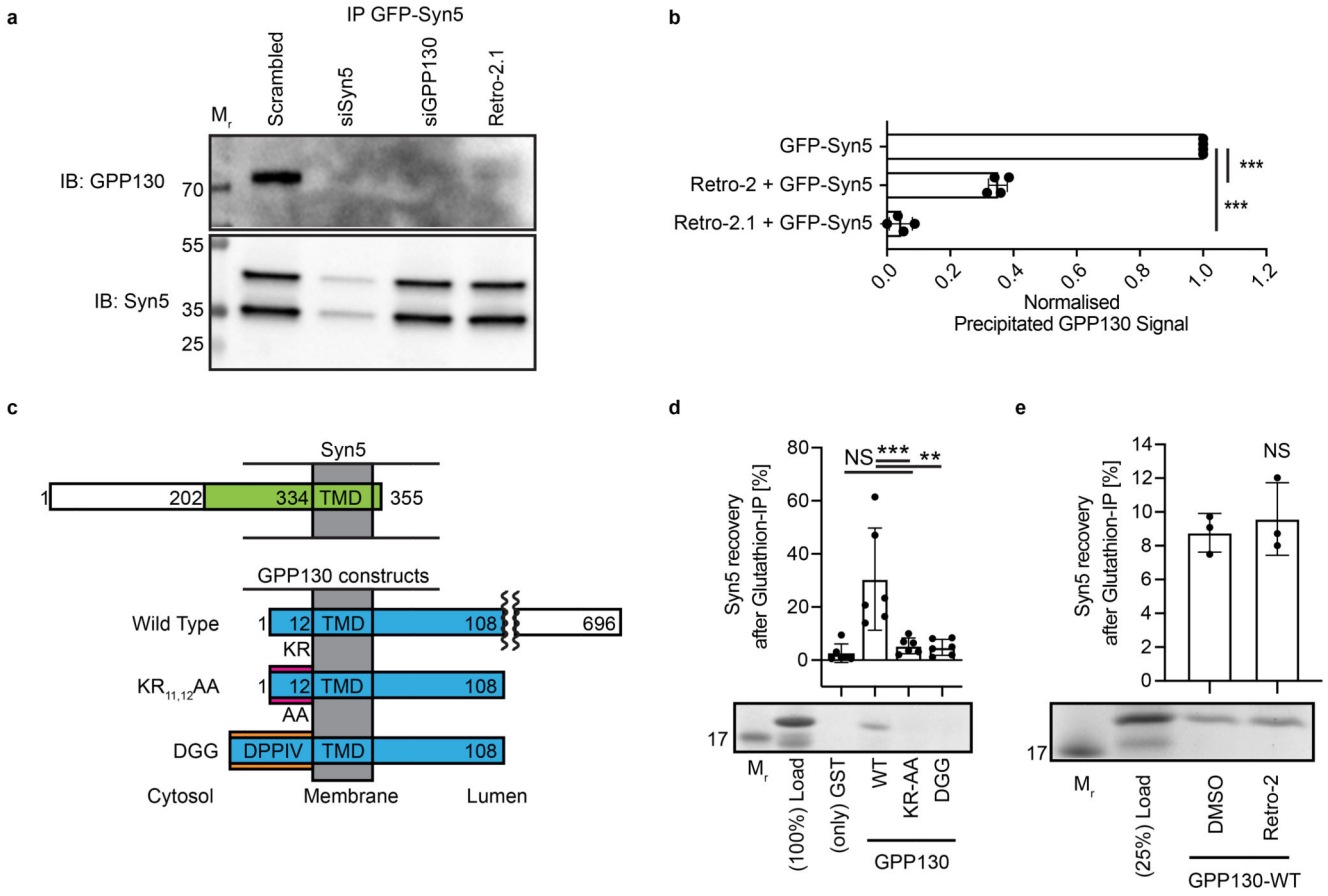

Figure 5. Syn5 interacts with GPP130.

(**a**) Western blotting of a representative GFP-Syn5 pull-down experiment in HeLa cells. GFP-Syn5 cells were treated with 0.05% DMSO (control), 25 μM Retro-2, or siRNAs against Syn5 or GPP130. Note that pull-down of GPP130 was only observed in the control condition. For Syn5, the double bands represent the two isoforms of the protein. Blot is representative of 4 independent repeats. See Supplementary Fig. 7c for full gels. (**b**) Quantification of GPP130 signals on western blots following GFP-Syn5 pull-down in the indicated conditions. Graph shows mean +/- SD each point represents one experiment, from 4 independent experiments. One-way ANOVA was performed overall ($P < 0.0001$) with Dunnett's multiple comparisons test comparing GFP-Syn5 to Retro-2 or Retro-2.1 treated. *** $P < 0.0001$. (**c**) Schematic representation of Syn5 and GPP130 constructs purified for *in vitro* binding studies. (**d**) Purified $Syn5_{202-355}$ was incubated with purified GST, GST-$GPP130_{1-108}$ (WT), GST-$GPP130_{1-108}$ with $KR_{11,12}AA$ substitution in the cytosolic domain, or GST-$GPP130_{1-108}$ with a substituted cytosolic domain from DPPIV (DGG). Anti-GST-beads were used to collect the complexes, recovery of $Syn5_{202-355}$ was determined by Coomassie staining of SDS-PAGE gels, and quantified from 6 independent experiments. Graphs show mean +/- SD, each point represents one experiment. Conditions normalized to total loaded protein (Load). One-way ANOVA was performed overall ($P < 0.0002$) with Sidak's multiple comparisons test. NS $P = 0.9925$, *** $P < 0.001$, ** $P = 0.0012$. See Supplementary Fig. 7d for full gels. (**e**) Experiment as in (d) in which the pull-down of

Europe PMC Funders Author Manuscripts

$Syn5_{202-355}$ by GST-$GPP130_{1-108}$ (GPP130-WT) was quantified in the presence of 25 μM Retro-2 or 0.05% DMSO. Graphs show mean +/- SEM, DMSO and Retro-2 conditions normalized to total loaded protein (Load). Paired two-tailed t-test comparing DMSO to Retro-2, NS P = 0.5. See Supplementary Fig. 7e for full gels.

Europe PMC Funders Author Manuscripts

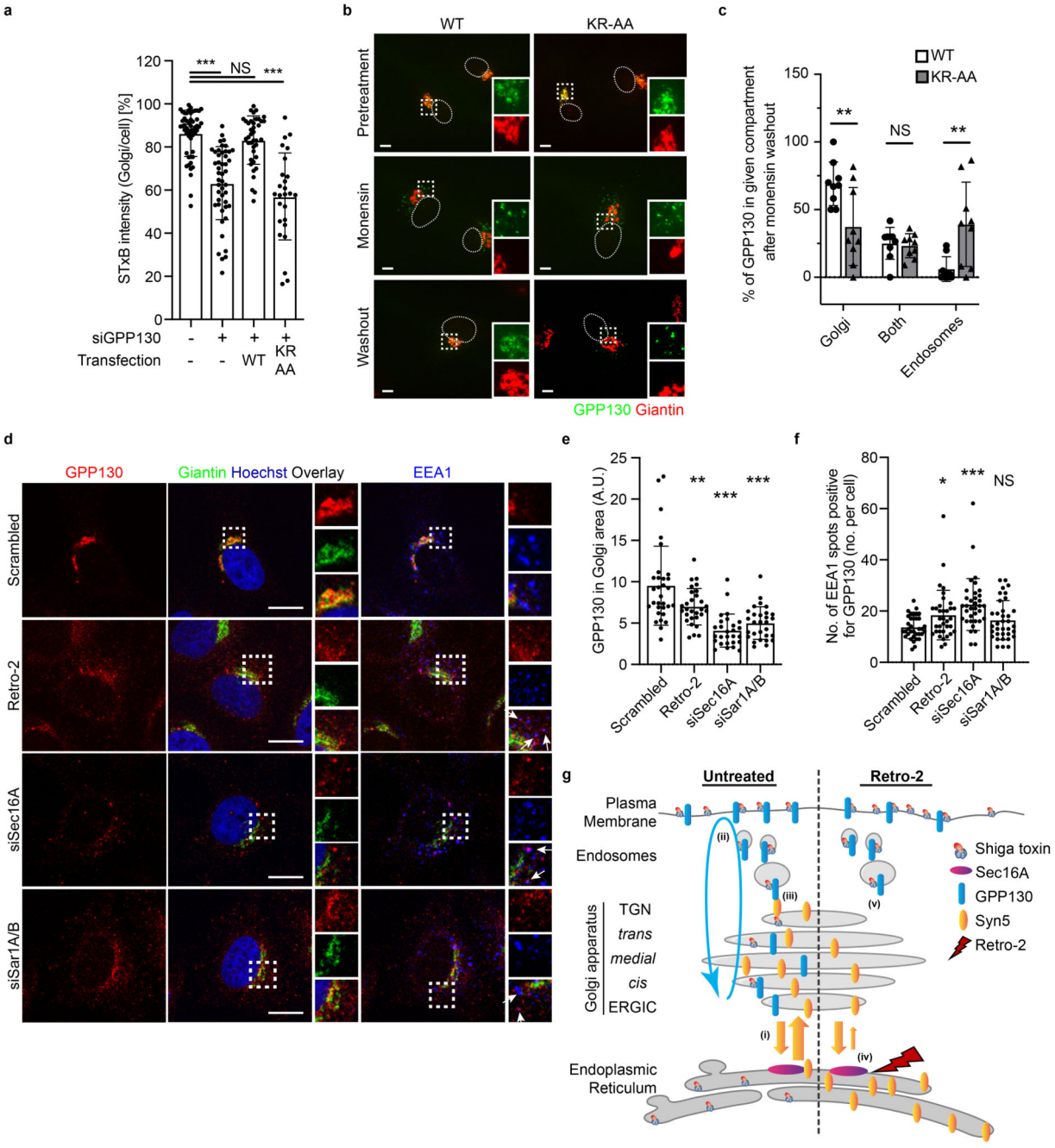

Figure 6. Syn5-GPP130 interaction is required for STxB retrograde trafficking.

(**a**) Retrograde trafficking of STxB in scrambled (-) or siGPP130 (+) treated cells. Where indicated, cells were transfected with siRNA resistant wild-type $GPP130_{1\text{-}108}$ (WT), or the KR/AA-mutant of $GPP130_{1\text{-}108}$. Quantification of STxB-Cy3 labeling in the Golgi area in the indicated conditions. Graph shows mean +/- SD for 52 (control), 47 (siGPP130), 39 (WT rescue), 29 (KR, AA rescue) cells from 2 out of 3 independent experiments. Each point represents a cell. One-way ANOVA was performed overall ($P < 0.0001$) with Sidak's multiple comparisons test. NS $P = 0.8903$, *** $P < 0.0001$. (**b**) Retrieval of GPP130 from

Europe PMC Funders Author Manuscripts

endosomes. Gene-edited cells lacking GPP130 were transfected with either HA-$GPP130_{1\text{-}108}$ (WT) or the KR/AA-GPP130 mutant construct. Cells were then harvested before treatment (pre-treatment), treated with monensin for 1 h to redistribute GPP130 to endosomes, or monensin-treated and then subjected to a 3 h washout. Cells were labeled with GPP130 (green) and giantin (red). Representative immunofluorescence images are shown from 9 independent experiments. Dotted lines indicate nuclei, dashed lines show areas of zooms. Scale bars = 10 μm. (**c**) Quantification of number of cells with GPP130 primarily Golgi-localized, a mix of Golgi- and endosome-localized, or primarily endosome-localized, in washout conditions for WT and KR-AA transfected cells in (b). Graph shows mean +/- SD of ~50 cells from 9 independent experiments. Two-way ANOVA was performed overall ($P < 0.0001$) with Sidak's multiple comparisons test. Golgi: ** $P = 0.0044$, Both: NS $P = 0.9925$, Endosomes ** $P = 0.0027$. (**d**) Redistribution of GPP130 in Retro-2, siSec16A, or siSar1A/B conditions. Confocal microscopy was performed for GPP130 (red), Giantin (green), EEA1 (blue in right panels) and Hoechst (blue in left panels). Dotted lines indicate zoomed areas. Arrows indicate GPP130 spots colocalizing with EEA1-positive vesicles. Scale bars = 10 μm. Representative images from 3 independent experiments. (**e**) Quantification of GPP130 in Golgi area as defined by giantin. Graph shows mean +/- SD for 31 (Scrambled), 29 (Retro-2), 27 (siSec16A), 29 (siSar1A/B) cells from 2 out of 3 independent experiments. Each point represents one cell. One-way ANOVA performed overall ($P < 0.0001$) with Dunnett's multiple comparisons test comparing all conditions to scrambled, Retro-2: ** $P = 0.0044$, siSec16A/siSar1A/B: *** $P < 0.0001$. (**f**) Quantification of GPP130 in EEA1 positive structures. Graph shows mean +/- SD for 35 cells per condition from 2 out of 3 independent experiments. Each point represents a cell. One-way ANOVA performed overall ($P < 0.0002$) with Dunnett's multiple comparisons test comparing all conditions to scrambled, Retro-2: * $P = 0.048$, siSec16A: *** $P < 0.0001$, siSar1A/B NS $P = 0.3654$. (**g**) Schematic model of Retro-2's mode of action. (i) Under untreated conditions, Syn5 cycles in a Sec16A-dependent manner between Golgi and ER. (ii) GPP130 cycles between Golgi and plasma membrane. (iii) In this study, we show that GPP130 and Syn5 interact directly, and that this interaction is involved in Shiga toxin trafficking from endosomes to the Golgi. (iv) Retro-2 binds to Sec16A, reducing anterograde Syn5 trafficking, thereby leading to its relocalization to the ER. (v) Syn5 relocalization prevents its interaction with GPP130 and results in the inhibition of retrograde Shiga toxin trafficking.